Bone 117 (2018) 98–115

Contents lists available at ScienceDirect

Bone

journal homepage: www.elsevier.com/locate/bone

Full Length Article

Glucose dependent miR-451a expression contributes to parathyroid hormone mediated osteoblast differentiation

Anirudha Karvande, Priyanka Kushwaha, Naseer Ahmad, Sulekha Adhikary, Priyanka Kothari, Ashish Kumar Tripathi, Vikram Khedgikar, Ritu Trivedi*

Division of Endocrinology, Central Drug Research Institute (Council of Scientific and Industrial Research), Sector 10, Jankipuram Extension, Sitapur Road, Lucknow 226031, Uttar Pradesh, India

ARTICLE INFO

Keywords:
PTH
Glucose
AMPK
Osteoblast differentiation
MicroRNA

ABSTRACT

Parathyroid hormone (PTH; amino acid 1–34, known as teriparatide) has reported promoting differentiation and glucose uptake in osteoblasts. However, how PTH regulates glucose metabolism to facilitate osteoblast differentiation is not understood. Here, we report that PTH promotes glucose dependent miR-451a expression which stimulates osteoblast differentiation. In addition to glucose uptake, PTH suppresses AMPK phosphorylation *via* PI3K-mTOR-AKT axis thereby preventing phosphorylation and inactivation of octamer-binding transcription factor 1 (OCT-1) which has been reported to act on the promoter region of miR-451a. Modulation of AMPK activity controls miR-451a levels in differentiating osteoblasts. Moreover, pharmacological inhibition of PI3K-mTOR-AKT axis suppressed miR-451a *via* increased AMPK activity. We report that this glucose regulated miRNA is an anabolic target and transfection of miR-451a mimic induces osteoblast differentiation and mineralization *in vitro*. These actions were mediated through the suppression of Odd-skipped related 1 (Osr1) and activation of Runx2 transcription. When injected *in vivo*, the miR-451a mimic significantly increased osteoblastogenesis, mineralization, reversed ovariectomy induced bone loss and improved bone strength. Together, these findings suggest that enhanced osteoblast differentiation associated with bone formation in case of PTH therapy is also a consequence of elevated miR-451a levels *via* glucose regulation. Consequently, this miRNA has the potential to be a therapeutic target for conditions of bone loss.

1. Introduction

Parathyroid hormone (PTH; amino acid 1–34, known as teriparatide), with the intermittent treatment regimen, is known to increase bone formation and reduce fracture incidences in osteoporotic patients [1]. Skeletal studies based on PTH therapy show its bone anabolic effects through monitoring osteoblast cells at multiple levels; these include enhancement of osteoblast activity, promotion of osteoblast differentiation, reduction of osteoblast apoptosis, and stimulation of quiescent bone-lining cells [2–5]. Research has shown that elevated serum glucose levels observed in diabetes affect bone metabolism [6]. In response, intermittent PTH treatment has improved bone mineral density and led to a reduction in serum glucose levels and [6,7]. At the cellular level, PTH and insulin-like growth factor I (IGF-1) stimulate glucose transport in osteoblastic cells and promote expression of Glut1 which is an important glucose transporter effective during skeletogenesis [8,9]. In particular, PTH shows its bone anabolic effect by stimulating aerobic glycolysis while suppressing glucose oxidation under the regulation of IGF-1–phosphatidylinositol-3-kinase (PI3K)–mammalian target of rapamycin (mTOR) signaling [10]. Importantly, PTH enhances IGF-1 levels in osteoblast cells [11] and inhibition of either IGF-1 or IGF-1 receptor hampers PTH mediated bone anabolic effect [12]. However, potential application in bone pharmacotherapy demands exploration of additional mechanisms in PTH mediated bone

Abbreviations: Ovx, Ovariectomy; PTH, Parathyroid Hormone; miRNA, MicroRNA; μCT, Micro-computed tomography; BMD, Bone mineral density; BV/TV, Bone volume/Total volume; SMI, Structural model index; Tb.N, Trabecular number; Conn Dn, Connection density; Tb.Sp, trabecular separation; ALP, Alkaline phosphatase; Runx-2, Runt-related transcription factor 2; Osr1, Odd-skipped related 1; AMPK, 5′ Adenosine monophosphate-activated protein kinase; PI3K, Phosphatidylinositol-4,5-bisphosphate 3-kinase; mTOR, Mammalian target of rapamycin; OCT-1, Octamer-binding transcription factor-1; BMP-4, Bone morphogenetic protein-4; p27, Cyclin-dependent kinase inhibitor-1B; AICAR, 5-Aminoimidazole-4-carboxamide ribonucleotide; Comp C, Compound C or Dorsomorphin; IGF-1, Insulin like growth factor-1; MCO, Mice calvarial osteoblast; siScr, Scrambled siRNA; miR-C, miRNA-control; 2-DOG, 2-Deoxyglucose; BMCs, Bone marrow cells

* Corresponding author.
E-mail address: ritu_trivedi@cdri.res.in (R. Trivedi).

https://doi.org/10.1016/j.bone.2018.09.007
Received 27 March 2018; Received in revised form 7 September 2018; Accepted 11 September 2018
Available online 13 September 2018
8756-3282/

anabolism.

Lactation and weaning are the important phases of a female reproductive system coupled with bone resorption and formation respectively. Postweaning phase is the most bone anabolic phase where bone loss during lactation is completely regained [13]. Earlier reports evidenced the link between the postweaning rise in PTH levels and skeletal recovery [14,15]. Previously we evidenced the up-regulation of a limited cohort of micro-RNAs (miRNAs) through miRNA profiling during late weaning phase [16]. Of the various candidates, one miRNA of potential interest is miR-451a. miR-451a has been well studied for its role as a tumor suppressor in osteosarcoma and found to be up-regulated during fracture healing as well as postnatal skeletal recovery [17–20]. Additionally, miR-451a transcription shows glucose dependency and found to be suppressed after AMPK activation during glucose deprivation in glioblastoma cells [21–23]. Since, both PTH and miR-451a show elevated expressions during late weaning phase and helping in fracture repair, we hypothesized that there might be a possibility of the existence of a regulation between them in context to skeletal recovery.

To validate this observation, we examined miR-451a expression during therapeutic intermittent PTH regimen in ovariectomized mice, where osteoblast activity is increased by PTH resulting in restoration of trabecular network. Our study showed that the glucose regulated miR-451a expression which is in turn modulated specifically by PTH during osteoblast differentiation. We further investigated miR-451a action on the osteoblasts both *in vitro* and *in vivo*. Odd-skipped related 1 (Osr1) was identified as a direct target of miR-451a. miR-451a mimic represses Osr1 and promotes the BMP-4 induced osteoblast differentiation and thus bone formation. Through this study, we could establish that PTH regulates glucose dependent miR-451a that in turn increases osteoblast differentiation and finally bone formation.

2. Materials and methods

2.1. Chemicals and reagents

The miRNA isolation kit (miR-Vana), miR-451a mimic, miR-451a inhibitor, miR-control, Osr1 and OCT-1 siRNA, scrambled siRNA were purchased from Ambion (Life Technologies, USA), and the BMP-4 ELISA was from Chongqing Biospes Co., Ltd. (China). Human PTH (1–34), D-Glucose, Compound C and AICAR were purchased from Calbiochem - Merck Millipore, Germany. LY294002 and AKT 1/2 inhibitor were purchased from Sigma-Aldrich, St. Louis, USA. WZB 117 was purchased from Tocris bioscience, UK. StepOne real-time PCR system and a TaqMan 5 nuclease probe method (Applied Biosystems, California, USA) were used to perform Quantitative PCRs. miRNA transcripts were normalized to U6 [16,24].

2.2. miRNA target site prediction and transfection studies in osteoblast cells

In silico putative targets were screened for miR-451a using TargetScan and miRanda on the basis of specific base-pairing rules [16,25,26]. The mature type of miR-451a; a mimic (Assay ID: MC10286 Applied Biosystems; sequence of miR-451a-AAACCGUUACCAUUAC UGA-GUU) which shows activity similar to endogenous mature miRNA and its antisense called anti-miR-451a; an inhibitor (Assay ID: MH10286, Applied Biosystems; sequence-AACUCAGUAAUGGUA-ACG GUUU) were transfected by using cationic liposomes (Lipofectamine RNAiMAX) according to the manufacturer's lipofection protocol. Transfections of the mimic and inhibitor into mouse osteoblasts were carried out at 50–60% confluence with reduced-serum and antibiotic-free OptiMEM using the transfection agent (Invitrogen). Knockdown experiments for Osr1 (Assay ID-s76718), OCT-1 (Assay ID-68746) were performed using the same protocol as above. ALP activity, mineralization, and qPCR were performed using protocols published previously [16].

2.3. Calvarial cell culture and alkaline phosphatase assay

For experiments, 1-day-old mice calvarial osteoblasts (MCOs) were used, harvested from nine to ten calvariae at room temperature. Initially, individual calvariae were isolated from the skull surgically followed by separating the sutures and the pooled calvariae were kept for repetitive digestion (15 min/digestion) with 0.05% trypsin and 0.1% collagenase P to release cells. The first digestion supernatant was discarded. The supernatant containing cells were collected from the next four digestions in 2 ml fetal bovine serum FBS and centrifuged. Cells were cultured in α-minimum Eagle's medium (Gibco, USA) containing 10% FBS and 1% penicillin/streptomycin (complete growth medium). Calvarial osteoblasts were allowed to reach 70–80% confluence for the experiments [16].

For the measurement of alkaline phosphatase (ALP) activity, MCOs at ~80% confluence were trypsinized and 2×10^3 cells per well were seeded in 96-well plates. Cells were transfected and incubated for 48 h in α-MEM supplemented with 5% charcoal treated FBS, 10 mM β-glycerophosphate, 50 $\mu g \cdot ml^{-1}$ ascorbic acid, and 1% penicillin or streptomycin (osteoblast differentiation medium). At the end of the incubation period, total ALP activity was measured using *p*-nitrophenyl phosphate (PNPP) as substrate and absorbance was read at 405 nm using SpectraMax Paradigm Multi well Elisa plate reader (Molecular Devices) [27].

2.4. Mineralization assay

MCOs were seeded on to 12-well plates (10,000 cells per well) in osteoblast differentiation medium. MCOs were transfected with or without miR-C, miR-451a, Anti-miR-451a, siScr or siOsr1, incubated for 21 days. Media were changed and transfection was performed after every 48 h. At the end of the experiment, cells were washed with phosphate-buffered saline (PBS) and fixed with 4% paraformaldehyde in PBS for 15 min. The fixed cells were stained with alizarin red-S (ARS) (40 mM, pH 4.5) for 30 min followed by washing with tap water. Stained cells were first photographed under a light microscope, and alizarin stain S was then extracted by using 10% (v/v) acetic acid with shaking at room temperature for 30 min. Cells were scrapped out from wells and centrifuged (2000*g* for 15 min), and the supernatant was collected. To the supernatant, 10% (v/v) ammonium hydroxide was added to bring the pH of the solution to 4.5 for colour formation. Absorbance of the solution was read at 405 nm [28].

At the end of the treatments, bone marrow cells (BMCs) from the femora of mice were flushed out in osteoblast medium containing α-MEM supplemented with 5% charcoal treated FBS, 10 mM β-glycerophosphate, 50 $\mu g \cdot ml^{-1}$ ascorbic acid and 1% penicillin or streptomycin (osteoblast differentiation medium) and 10^{-7} M dexamethasone (bone marrow differentiation medium). BMCs were cultured for 21 days and mineralized nodules were stained and quantified as described above [29].

2.5. Quantitative real-time PCR (qPCR)

Cells were collected in 1 ml of TRIzol reagent (Invitrogen), and total RNA was extracted according to the manufacturer's protocol. cDNA was synthesized using Revert Aid First Strand cDNA synthesis kit (No.K1621 Fermentas, Burlington, ON, Canada) from 1 μg of total RNA. Quantitative real-time PCR amplifications were performed in the Light Cycler 480 Real-Time PCR System (Roche Diagnostics, Indianapolis, IN, USA) using Light Cycler SYBR Green (Roche Diagnostics) according to the manufacturer's instruction. The sequences of primer sets for Osr1, p27, BMP-4, Runx2, OCT-1 and β-actin are shown in Table 1. The quantity of each sample was normalized using the CT (threshold cycle) value obtained for the β-actin mRNA amplifications [16].

Table 1
Primer sequence of various genes used for qPCR.

Gene symbol	Primer sequence	Accession no.
β-Actin	F-CTAAGGCCAACCGTGAAAAG R-ACCAGAGGCATACAGGGACA	NM_007393.5
BMP-4	F-GAGGAGTTTCCATCACGAAGA R-GCTCTGCCGAGGAGATCA	NM_007554.3
Runx2	F-GCCCAGGCGTATTTCAGA R-TGCCTGGCTCTTCTTACTG	NM_001145920.2
Osr1	F-AGAAGCGTCAGAAGTCTAGTTCG R-GGAACCGCAATGATTTCAA	NM_011859.3
p27	F-GTTAGCGGAGCAGTGTCCA R-TCTGTTCTGTTGGCCCTTTT	NM_009875.4
OCT-1	F-GTGCTGCTGTGACTAATCTCTCTC R-TGGTGGTGACTCTGTCTGGT	NM_198934.3

qPCR, quantitative polymerase chain reaction; F, forward; R, reverse.

2.6. Western blot analysis

MCOs were grown to 80% confluency followed by various treatments for respective time periods. Cells were washed with cold phosphate-buffered saline (vehicle), and whole-cell lysates were prepared by the addition of lysis buffer from Sigma-Aldrich containing a protease inhibitor and phosphatase inhibitor mixture from Sigma-Aldrich. Femur was crushed in liquid nitrogen and lysis buffer followed by centrifugation [16]. Protein content was quantified by BCA method. Protein (30–50 μg) was loaded per lane and separated on a 10% polyacrylamide gel, followed by transfer to a PVDF membrane (Millipore, Billerica, MA, USA) by electroblotting. Membrane was blocked with 5% non-fat dry milk and followed by incubation with a primary antibody at 4 °C overnight. OCT-1, Osr1, mTOR, p-mTOR, Runx2, AMPK (Abcam, Cambridge, MA, USA), β-Actin, BMP-4, PI3K, p-PI3K (Santa Cruz), p-AMPK(T172), AKT, p-AKT(S473) (Cell Signaling, USA) and Anti-phospho-OCT1 (S335) Octamer-binding transcription factor 1; a gift from Dean Tantin, University of Utah; peptide antigen used – (RFEALNLsFKNMCKL) Membranes were washed and were probed with a horseradish peroxidase (HRP)-conjugated secondary antibody (Cell Signaling, USA) and visualized by an enhanced chemiluminescence system (GE Healthcare Life Sciences, Bangalore, India) according to the manufacturer's instructions [16]. Densitometry was performed using ImageJ software as previously described [30].

2.7. Immunocytochemistry

MCOs were incubated in medium with or without miR-451a mimic and anti-miR-451a and were grown in Lab-Tek Chamber Slides (Nunc, Denmark) for 48 h. For immunocytochemistry, cells were fixed with 4% paraformaldehyde (PFA) followed by permeabilization with 0.1% Triton X-100 and incubation in primary antibody (Runx2-mouse monoclonal antibody 1:100 dilution) for overnight. Alexa Fluor 488 goat anti-mouse (Invitrogen, USA) was used as secondary antibody. Slides were mounted with ProLong™ Gold Antifade Mountant with DAPI (Life Technologies, USA). Fluorescence was captured using a fluorescent microscope (Eclipse 80i, Nikon, Tokyo, Japan) with the aid of appropriate filter (excitation 490 nm and emission 525 nm) [31].

2.8. [3H] 2-Deoxyglucose uptake assay

The MCOs were cultured in 24-well plates till 70–80% confluence. Cells were treated with PTH (500 $ng \cdot ml^{-1}$) for 48 h in differentiation medium. Washing followed by incubation was performed with serum-free medium. Cells were incubated with Insulin (10 nM) for 30 min followed by washing with HEPES saline (pH 7.4). This is followed by incubation with 250 μl of KRH buffer (20 mM HEPES, pH 7.4, 136 mM NaCl, 4.7 mM KCl, 1.25 mM $MgSO_4$, and 1.25 mM $CaCl_2$) containing mixture of 5 mCi of 2-[1,2-^{3}H]-deoxy-D-glucose and 1 mM of 2-Deoxy Glucose (2-DOG; MP Biomedicals, California, USA) and left for 5 min. The reaction was terminated by adding stop solution (200 mM of 2-DOG) followed by two times washing with ice-cold PBS. Cells were scrapped in of 0.5 M NaOH (500 μl per well) and collected in scintillation vials containing 5 ml of cocktail W scintillation grade (Sisco Research Laboratories Pvt. Ltd., Mumbai, India). Radioactivity retained by the cell lysate was measured by a liquid scintillation counter (Beckman Coulter, LS 6500, and Beckman Coulter Inc. USA) [32].

2.9. In vivo studies and assessment of bone parameters

The study was carried in accordance with current legislation on animal experiments (Institutional Animal Ethical Committee at Central Drug Research Institute, Approval Reference no. - IAEC/2017/F-235) and performed according to the regulations of the Council for the Purpose of Control and Supervision of Experiments on Animals, Ministry of Social Justice and Empowerment, Government of India. Female 8 weeks old BALB/c mice (18 ± 5 g) were kept in a 12-h light-dark cycle with controlled temperature (22–24 °C) and humidity (50–60%) and *ad libitum* access to standard rodent food and water [16]. The subcutaneous dose for PTH (40 $\mu g \cdot kg^{-1}$ for 5 $days \cdot week^{-1}$) used in this study is shown to have an anabolic effect [33]. Micro-computed tomography (μCT) measurements were carried out on a SkyScan 1076 CT scanner (Aartselaar, Antwerp, Belgium). miR-451a mimic and miR-C were administered (7 $mg \cdot kg^{-1}$ each) through tail vein injection [16,34] with an anionic liposome (Invivofectamine 3.0, Life Technologies) which allows for the fusion of the liposome-nucleic acid complex with the cell membrane and subsequent uptake by endocytosis. Various treatments were started 6 weeks after the ovariectomy and continued for 6 weeks. Precisely, injections were given on 1st, 2nd and 3rd days of 1st, 3rd and 5th weeks. After 6 weeks of treatment, all mice were sacrificed and autopsied to collect femur (measurement of the bone parameter) and organs like liver, kidney and uterus. Blood was collected to separate serum and stored at −80 °C for further experiments. Bone marrow cells (BMCs) from femurs of vehicle and treatment groups mice were harvested, and mineralization was studied as described previously [29]. Briefly, femora were scanned at a nominal resolution of 18 mm. One hundred projections were acquired (angular range, 180°) and image slices were reconstructed using a modified Feldkamp algorithm (according to Sky Scan Nrecon software). Parameters, including bone volume-to-tissue volume (BV/TV), trabecular number (Tb.N), and trabecular separation were calculated [16,29]. Femora were subjected to three-point bending using a bone strength tester (model TK-252C; Muromachi Kikai, Co. Ltd., Tokyo Japan) [16].

To check the integrity of the trabecular region, 6 μm undecalcified sections were prepared from distal femur metaphysis and embedded in polymerized methyl methacrylate. For osteoblast and osteoclast/bone resorption examination Goldner trichrome, Toluidine blue, Von Kossa and TRAP staining were performed according to the protocol available from Bioquant [35,36]. Total trabecular bone volume was measured by using Bioquant Osteo Software (Bioquant Image Analysis, Nashville, TN, USA).

2.10. Immunohistochemistry

Immunohistochemistry was performed to examine the expression level of Osr1 and Runx2 in the trabecular region of decalcified distal femur metaphysis. Femurs were fixed in 4% paraformaldehyde in 0.1 M PBS (pH 7.4). Fixed bones were decalcified by immersion in decalcifying solution lite (Sigma-Aldrich, St. Louis, USA) for 1 week and embedded in paraffin. 5 μm thick paraffin-embedded longitudinal bone sections were then blocked by 5% goat serum for 1 h at room temperature and incubated overnight with the primary antibodies (Osr1-rabbit monoclonal antibody 1:100 dilution and Runx2-mouse monoclonal antibody 1:100 dilution). Sections were then incubated with FITC goat anti-rabbit and Cy3 goat anti-mouse secondary antibodies

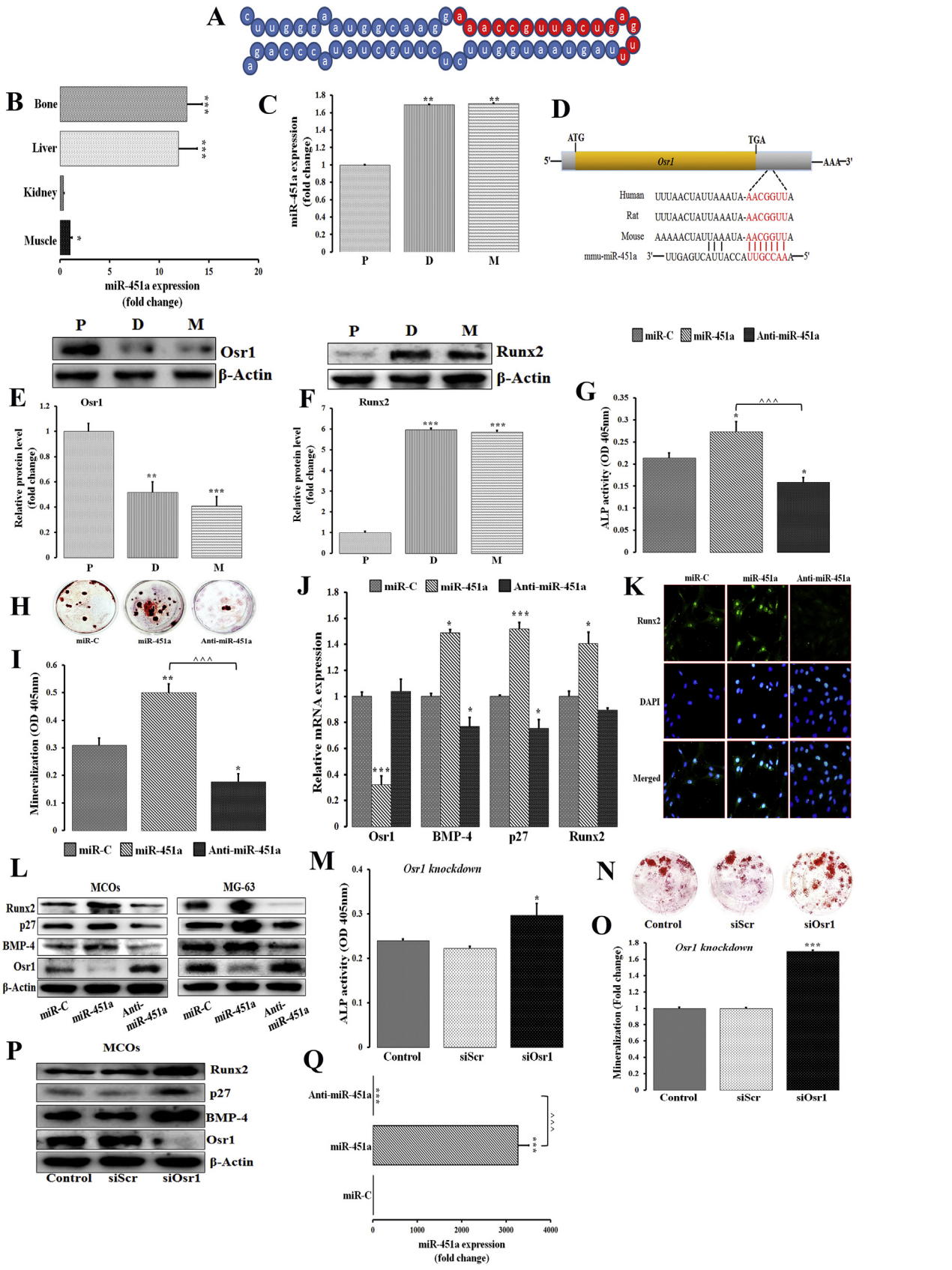

(caption on next page)

Fig. 1. miR-451a suppresses Osr1 to stimulate osteoblast differentiation. (A) Secondary structure of pre-miR-451a predicted by miR-base (mature miR-451a sequence shown in red). (B) Expression (qPCR) of miR-451a in different tissues. (C) Expression (qPCR) of miR-451a in osteoblasts during proliferation (P), differentiation (D) and mineralization (M). ($n \geq 3$) (D) *In silico* identification of the miR-451a target using the seed sequence to the 3′ UTR of Osr1 (red: conserved seed sequence in mammals). (E–F) Western blotting and its quantification for the expression of target protein Osr1 (E) and Runx2 (F) were performed in osteoblasts at proliferation, differentiation and mineralization stage; ($n \geq 3$). (G-L) Transfection experiments in osteoblasts with mimic or anti-miR-451a (50 nM each) on alkaline phosphatase (ALP) activity (G), representative wells showing alizarin-positive colony (Cfu-ob) formation in osteoblast cells cultures at day 15 in osteogenic medium (H) and quantification (I); ($n \geq 3$), quantitative PCR for the expression of target gene Osr1 and osteoblast differentiation genes, BMP-4, p27 and Runx2 at 48 h (J); ($n \geq 3$), immunofluorescence microscopy for Runx2 (K) (magnification-20×); ($n \geq 3$), western blotting for the expression of Osr1 and osteoblast differentiation genes, BMP-4, p27 and Runx2 at 48 h (L); ($n \geq 3$). (M–P) Knockdown experiments in osteoblasts with siRNA against Osr1 or scrambled siRNA (50 nM each) for alkaline phosphatase (ALP) activity (M); (OD at 405 nm, $n \geq 3$), alizarin-positive colony (Cfu-ob) (N), quantitation (O); (OD at 405 nm, $n \geq 3$) and western blotting (P) for the expression of BMP-4, p27 and Runx2 in osteoblasts. (Q) Expression (qPCR) of miR-451a after 21 days of transfection in MCOs. ($n \geq 3$). Data represented as Mean ± S.E.M. from three independent experiments; $^{*}p < 0.05$, $^{**}p < 0.01$, $^{***}p < 0.001$ compared with control; other comparison, $^{\wedge\wedge\wedge}p < 0.001$. (For interpretation of the references to colour in this figure legend, the reader is referred to the web version of this article.)

(Invitrogen, USA) for 1 h at room temperature. Sections were washed with PBS and mounted with ProLong™ Gold Antifade Mountant with DAPI (Life Technologies, USA). Fluorescence was captured using a confocal microscope (Carl Zeiss LSM510 Meta) with the aid of appropriate filter [37].

2.11. Statistical analysis

For experiments requiring multiple comparisons testing, we used one-way ANOVA followed by Newman-Keuls test of significance (GraphPad Prism v.5). Student's *t*-test was used for experiments with only two treatments [16].

3. Results

3.1. miR-451a drives osteoblast differentiation by regulating Osr1

The highly conserved miR-451a is identified earlier at the late weaning phase in the reproductive window [16]. It is located on human chromosome 17 in the noncoding region and forms a characteristic miRNA precursor stem-loop secondary structure (Fig. 1A). Tissue specific miRNA profiling showed miR-451a expresses significantly high in bone and liver compared with skeletal muscle or kidney (Fig. 1B). Furthermore, miR-451a expression increased significantly during osteoblast differentiation as well as in the mineralization phase (~2 fold) (Fig. 1C). In our attempt to predict the target for miR-451a using TargetScan and miRBase, Odd-skipped related 1 (Osr1) was confirmed as the putative targeted gene. Osr1 showed an 8-nt seed sequence match with miR-451a in the 3′ UTR and was highly conserved among vertebrates (Fig. 1D) [38,39]. Further, we confirmed the differential expression pattern of miR-451a during proliferation, differentiation and mineralization by western blotting for its putative target Osr1. During proliferation stage, Osr1 showed maximum expression while Runx2 showed decreased expression. Osr1 expression decreased gradually as cell started differentiation and mineralization while Runx2 increased concurrently (Fig. 1E–F). Transient transfection of MCOs with the miR-451a mimic stimulated osteoblast differentiation, ALP activity and mineralization along with increased mineralized nodules. In contrast, anti-miR-451a (a specific blocker for miR-451a) significantly reduced ALP activity and mineralization nodules (Fig. 1G–I). Quantitative PCR (q-PCR) showed increase in BMP-4, p27 and Runx2 expression with the miR-451a mimic transfection in MCOs cultures, while the modest inhibitory effects were noted with the anti-miR transfection (Fig. 1J). In concordance with the *in silico* data, we found that the miR-451a mimic repressed Osr1 expression, whereas Osr1 expression increased with anti-miR transfection. Immunofluorescence microscopy confirmed an increase in Runx2 expression in MCOs transfected with miR-451a mimic while a decrease in Runx2 protein expression with anti-miR-451a (Fig. 1K). These changes were further corroborated at the protein level by western blotting (Fig. 1L). To extrapolate this study in humans, human osteoblast-like cells – MG-63 were transfected with miR-451a mimic and anti-miR. Similar results were observed in MG-63 as seen in MCOs (Fig. 1L). Taken together, the results suggest that miR-451a directly promotes osteoblast differentiation and mineralization.

We next examined whether Osr1 repression was a pre-requisite for miR-451a induced Runx2 activation leading to osteoblast differentiation. siRNA mediated knockdown of Osr1 in MCOs showed, increased ALP activity and mineralization compared with scrambled siRNA-transfected cells (Fig. 1M–O). Furthermore, the expression of Runx2, p27 and BMP-4, protein in Osr1-depleted cells were analyzed. A markedly increased expression of Runx2, p27 and BMP-4 proteins were observed (Fig. 1P). We next analyzed the miR-451a expression after 21 days of transfection in mice calvarial cells. miR-451a mimic transfection elevated the endogenous miR-451a levels by ~3000 folds while anti-miR-451a suppressed the endogenous miR-451a levels (Fig. 1Q). These data suggest that Osr1 down-regulation is critical for miR-451a induced Runx2 expression and osteoblast differentiation.

3.2. PTH promotes miR-451a expression via glucose regulation

Given that, miR-451a is dependent on glucose in hepatocytes and cancer cells [21–23,40], we tested the levels of mature miR-451a in MCOs cultured for 48 h at three different conditions; vehicle or 1 mM glucose (low glucose condition), 4.5 mM (physiological glucose condition) and 10 mM (high glucose condition). Medium was replenished every 12 h up to 48 h. Significant increase in miR-451a levels was observed in high glucose (10 mM) condition when compared with low glucose (1 mM) condition; whereas physiological range showed an intermediate effect (Fig. 2A). Further, MCOs were cultured for 48 h in three different regimens: G▲(+); continuously high glucose (medium replenished every 12 h), G▼(−); continuously low glucose, and GΔ; low glucose replenished at 24 h with high glucose medium (Fig. 2B). In continuous high glucose, the expression of miR-451a was high, while in low glucose it significantly dropped. miR-451a dependency on glucose was further confirmed when an increase in miR-451a levels was observed in the osteoblasts after the glucose replenishment (Fig. 2C). In order to check the glucose-sensitive response of miR-451a expression on its direct target Osr1, western blotting was performed. Notably, in high glucose conditions, the expression of Osr1 remained low while in low glucose it was significantly elevated. Moreover Osr1 level decreased after the supplementation of glucose. On the contrary, Runx2 expression showed an inverse pattern compared with Osr1 (Fig. 2D). These results suggest that the expression of miR-451 is intrinsically linked to glucose levels.

PTH therapy is known to lower blood glucose levels in osteoporotic women [6,7] may be because PTH promotes aerobic glycolysis in osteoblast cells [10]. Thus, we investigated the change in miR-451a expression pattern during PTH supplementation. In consistent with the previous report, 500 $ng{\cdot}ml^{-1}$ of PTH [10] on osteoblasts for 48 h, significantly enhanced glucose uptake as confirmed by [3H] 2-deoxyglucose (2-DOG) uptake assay (Fig. 2E). Dose-dependent increase in miR-451a expression was observed in MCOs during PTH treatment (Fig. 2F). We next checked whether the presence of glucose has any effect on PTH mediated miR-451a expression. Glucose showed the

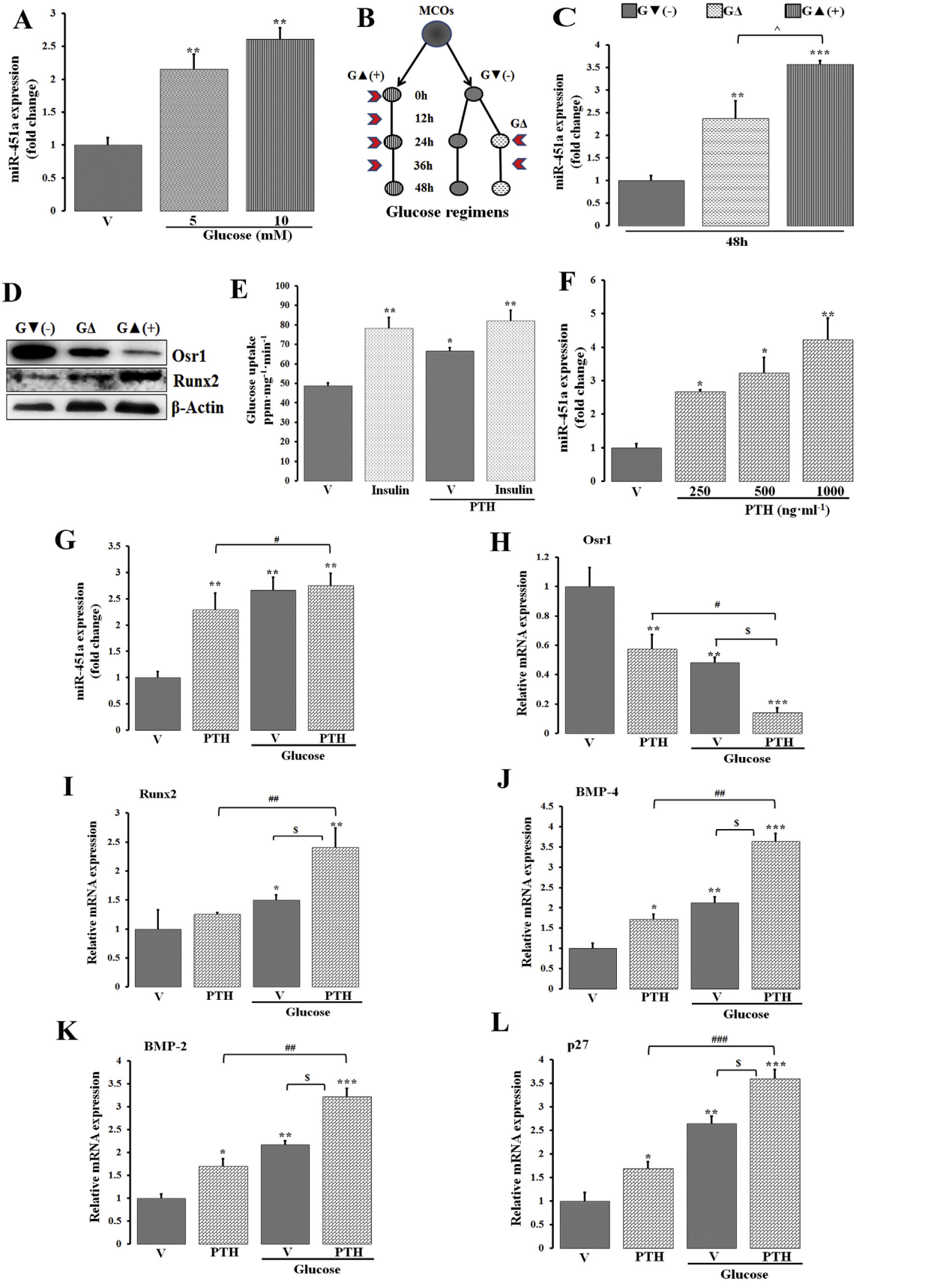

(caption on next page)

Fig. 2. PTH promotes miR-451a expression *via* glucose regulation. (A) Expression (qPCR) of miR-451a with different glucose concentrations in MCOs; ($n \geq 3$). (B–D) Glucose (10 mM) regimens used in the experiment; G▲(+); continuously high glucose, G▼(−); continuously low glucose and GΔ; low glucose replenished at 24 h with high glucose medium (B), expression (qPCR) of miR-451a expression in glucose regimens used (C); ($n \geq 3$) and western blotting showing the expression of target protein Osr1 and Runx2 in glucose regimens used in the experiment (D); ($n \geq 3$). (E) Glucose uptake in control and PTH (500 ng·ml^{-1}) treated osteoblasts for 48 h. The experiment was performed with or without acute insulin pulsing at 10 nM; ($n \geq 3$). (F–G) Expression (qPCR) of miR-451a was assessed with different PTH concentrations in MCOs (F); ($n \geq 3$) and glucose supplementation (10 mM) with PTH (500 ng·ml^{-1}) (G); ($n \geq 3$). (H-L) Quantitative PCR was performed for the expression of target gene Osr1 (H), Runx2 (I), BMP-4 (J), BMP-2 (K) and p27 (L) during osteoblast differentiation with or without glucose and PTH at 48 h; ($n \geq 3$). Data represented as Mean ± S.E.M. from three independent experiments; $^{*}p < 0.05$, $^{**}p < 0.01$, $^{***}p < 0.001$, compared with control; other comparisons, $\hat{}p < 0.05$, $\hat{}\hat{}p < 0.01$, $^{\#}p < 0.05$, $^{\#\#}p < 0.01$ and $^{\$}p < 0.05$.

additive effect to PTH mediated miR-451a expression, as revealed by quantitative real-time PCR assay (Fig. 2G). In agreement with the increase in miR-451a expression by PTH, Osr1 mRNA level was decreased whereas Runx2, BMP-4, BMP-2 and p27 transcripts were increased (Fig. 2H–L). Taken together, these data suggest that PTH promotes miR-451a expression *via* glucose uptake in osteoblast *in vitro*.

3.3. PTH promotes miR-451a mediated osteoblast differentiation by regulating AMPK activation

Provided that in low glucose conditions, activated AMPK phosphorylates and inhibits OCT-1 (a glucose regulated transcription factor) which in turn prevents miR-451a transcription in cancer cells [23]; we explored the involvement of PTH with this mechanism in osteoblasts. MCOs grown in low glucose conditions (vehicle) showed increased phosphorylation of AMPK (T172) and OCT-1 (S336) (complementary to OCT-1 at S335 in humans [23]) whereas in high glucose conditions decreased phosphorylation was observed, similar to cancer cells. Expression of downstream targets for miR-451a was further investigated to understand the association of miR-451a with the above mechanism in osteoblasts. Protein levels of Osr1 increased whereas, BMP-4, p27 and Runx2 levels decreased in low glucose conditions indicating decreased miR-451a levels and osteoblast differentiation (Fig. 3A).

Furthermore, PTH supplementation in MCOs decreased the phosphorylation of both AMPK as well as OCT-1 and their phosphorylation decreased further when PTH was supplemented in high glucose conditions (Fig. 3A). Similarly, to investigate the effect of PTH mediated AMPK inhibition on miR-451a levels, the expression pattern of downstream targets for miR-451a were analyzed. PTH markedly decreased the Osr1 levels and increased BMP-4, p27 and Runx2 protein levels indicating elevated miR-451a levels and osteoblast differentiation. Supplementation of glucose further boosted PTH mediated effect on these differentiation markers.

Pharmacological inhibition of AMPK activity by the small molecule inhibitor Compound C [41] resulted in the reduction of OCT-1 (S336) phosphorylation (Fig. 3A) with a simultaneous decrease in Osr1 levels leading to increasing miR-451a levels. *Vice versa* stimulation of AMPK by activator AICAR showed the opposite effects (Fig. 3A). In the agreement, we observed elevated BMP-4, p27, Runx2 levels in presence of Compound C while these proteins were suppressed in presence of AICAR. PTH supplementation along with Compound C or AICAR showed additive effects. These observations confirmed the involvement of PTH in AMPK inhibition leading to increased miR-451a expression and osteoblast differentiation. Furthermore, quantitative real-time PCR analysis showed increased miR-451a levels in the presence of AMPK inhibitor (compound C) while AMPK activator (AICAR) significantly alleviated miR-451a transcript (Fig. 3B). These results suggest that there might be possibility of existence of a mechanism for PTH by which it promotes miR-451a mediated osteoblast differentiation *via* inhibiting AMPK activation in presence of glucose. To confirm functional link between AMPK phosphorylation and osteoblast differentiation we treated MCOs with increasing concentration of AICAR for 48 h in differentiating medium. AICAR dose dependently elevated p-AMPK (T172) levels compared to untreated cells. AMPK phosphorylation was followed by OCT-1(S336) phosphorylation. AICAR treatment resulted in increased Osr1 levels along with decrease in Runx2, BMP-4 and p27 levels in dose dependent manner (Fig. 3C–D). These results suggest that reduction in p-AMPK (T172) levels were essential during osteoblast differentiation.

3.4. Glucose uptake favors PTH mediated inhibition of AMPK activation and osteoblast differentiation

To validate involvement of glucose uptake in PTH mediated suppression of AMPK phosphorylation and osteoblast differentiation, we treated MCOs with the glucose transporter inhibitor WZB 117 (Glut-i) which competitively inhibits GLUT 4, GLUT 1 and GLUT 3. Glucose alone and PTH supplemented with glucose significantly decreased p-AMPK (T172), p-OCT-1(336) and Osr1 levels and increased osteoblast differentiation markers Runx2, BMP-4 and p27 compared with the vehicle as concurrent with the previous results. Pharmacological inhibition of glucose transporters GLUT on osteoblast by addition of Glut-i resulted into inverse effects as observed in case of glucose and PTH supplemented with glucose conditions. Addition of Glut-i removed the inhibitory effect as observed in case of PTH supplemented with glucose and elevated p-AMPK, p-OCT-1 and Osr1 levels while inhibited osteoblast differentiation markers Runx2, BMP-4 and p27 (Fig. 4A–B). These findings suggest that glucose uptake is necessary for PTH mediated AMPK inactivation during osteoblast differentiation.

3.5. OCT-1 drives miR-451a expression and promotes osteoblast differentiation

Earlier, the possibility of OCT-1 in osteoblast differentiation has been reported but the exact mechanism was not known. To elucidate the role of OCT-1 or POU2F1 during osteoblast differentiation we examined whether OCT-1 repression was a pre-requisite for miR-451a induced Runx2 activation leading to osteoblast differentiation. siRNA mediated knockdown of OCT-1 in MCOs showed a significant decrease in miR-451a levels compared with scrambled siRNA-transfected cells (Fig. 5A). Quantitative PCR (q-PCR) showed an increase in Osr1 level while a decrease in BMP-4, p27 and Runx2 expression with the OCT-1 siRNA transfection in MCOs cultures (Fig. 5B). Furthermore, the expression of Osr1, Runx2, p27 and BMP-4 protein in OCT-1-depleted cells were analyzed. A markedly decreased expression of Runx2, p27 and BMP-4 proteins were observed thus inhibiting osteoblast differentiation (Fig. 5C–D). These findings suggest that OCT-1 is crucial for miR-451a expression and promotes osteoblast differentiation.

3.6. PTH promotes glucose mediated inhibition of AMPK activation by PI3K-mTOR signaling

Previously, PTH has been reported to promote glycolysis *via* PI3K-mTOR signaling [10]. The observed PTH mediated inhibition of AMPK in presence of glucose led us to examine the involvement of PI3K-mTOR signaling in miR-451a mediated osteoblast differentiation. Involvement of PI3K-mTOR signaling pathway was clearly observed in the inhibition of AMPK phosphorylation by PTH in presence of glucose (Fig. 6A, left panel). This was evident from significant decrease in relative phospho-AMPK (T172) levels with a simultaneous increase in relative p-PI3K, p-mTOR and p-AKT (S473) levels.

To further confirm this, we evaluated the signaling cascade in

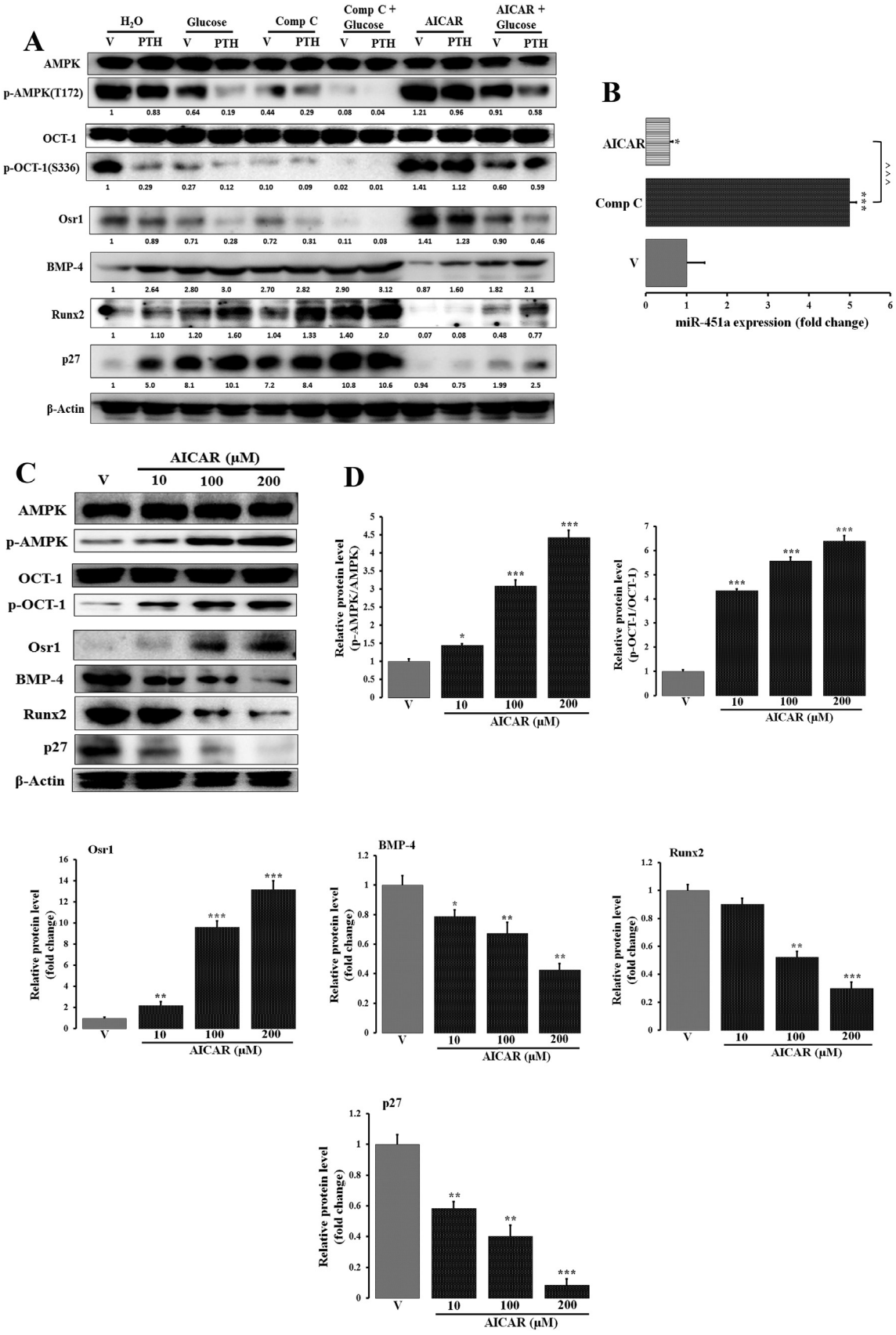

(caption on next page)

Fig. 3. PTH promotes miR-451a mediated osteoblast differentiation by regulating AMPK activation. (A) Western blotting showing the expression of phosphorylated and non-phosphorylated form of AMPK and OCT-1 along with target protein Osr1 and BMP-4, p27 and Runx2 in presence or absence of following: PTH (500 ng·ml^{-1}), glucose (10 mM), Compound C (1 μM) and AICAR (100 μM) in MCOs at 48 h. Densitometry analysis of respective proteins was performed using ImageJ software and the respective fold change was written below each gel; ($n \geq 3$). (B) Expression (qPCR) of miR-451a with compound C and AICAR in MCOs; ($n \geq 3$). (C) Western blotting showing the expression of phosphorylated and non-phosphorylated form of AMPK and OCT-1 along with target protein Osr1 and BMP-4, p27 and Runx2 with or without increasing concentration of AICAR (10, 100 and 200 μM). (D) Densitometry analysis of respective proteins was performed using ImageJ software; ($n \geq 3$). Data represented as Mean ± S.E.M. from three independent experiments; $^{*}p < 0.05$, $^{**}p < 0.01$, $^{***}p < 0.001$ compared with respective vehicle; other comparison, $^{\wedge\wedge\wedge}p < 0.001$.

presence of PI3K or AKT inhibitors, along with glucose and PTH supplementation. Inhibition of PI3K by LY294002 blocked PTH mediated AMPK inactivation. This was evident in the results showing no change in relative phosphorylation of AMPK and p-PI3K, p-mTOR and p-AKT (S473) levels (Fig. 6A, middle panel, B) in case of PI3K inhibition. Moreover, glucose supplementation along with PTH could not show any additive effect in presence of PI3K inhibitor. Inhibition of AKT phosphorylation by an AKT 1/2 inhibitor abolished the effects of PTH treatment and resulted in increased phosphorylation of AMPK in the presence or absence of glucose (Fig. 6A, right panel, C). Thus, PTH

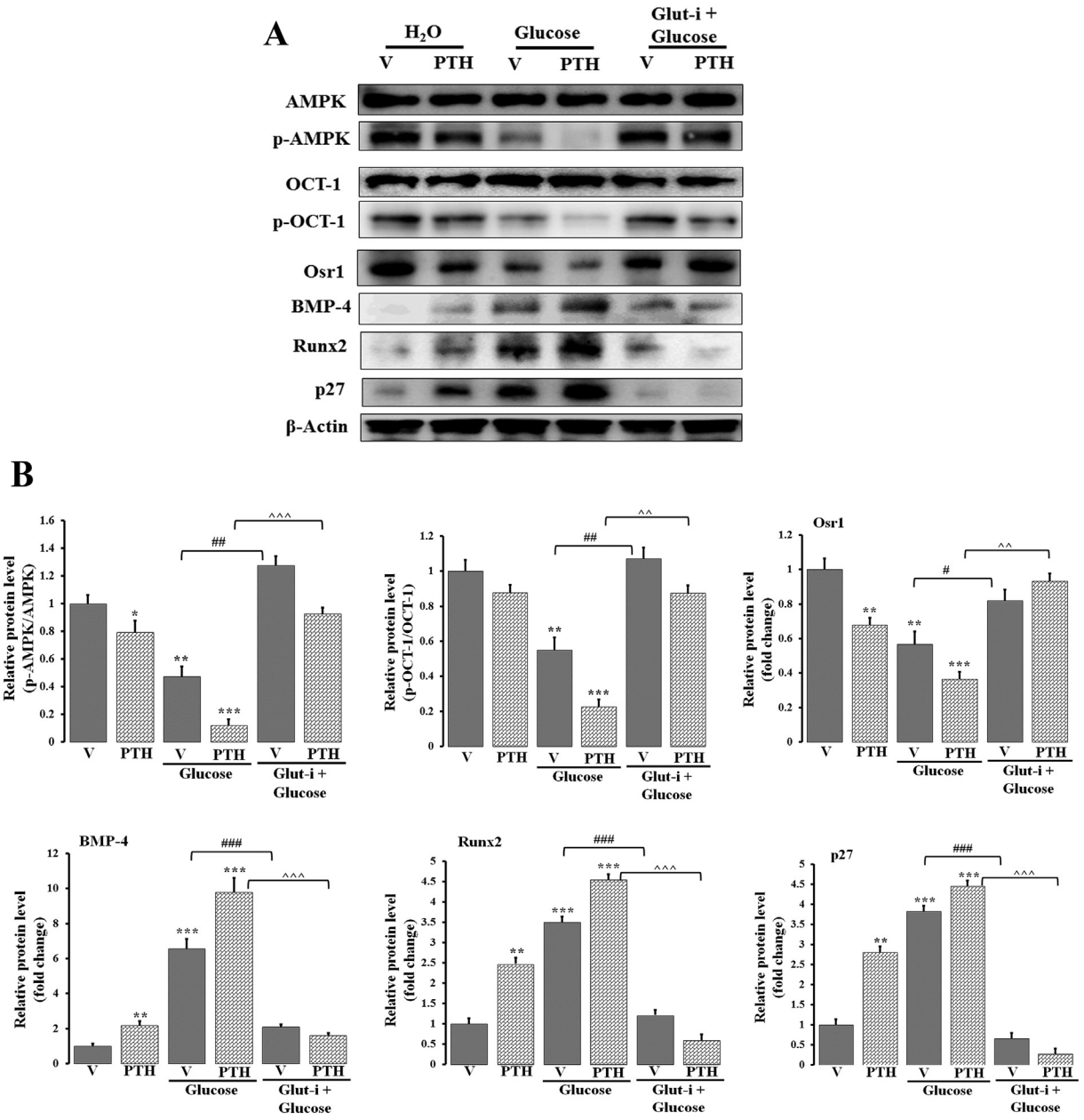

Fig. 4. Glucose uptake favors PTH mediated inhibition of AMPK activation and osteoblast differentiation. (A) Western blotting showing the expression of phosphorylated and non-phosphorylated form of AMPK and OCT-1 along with target protein Osr1 and BMP-4, p27 and Runx2 in presence or absence of following: PTH (500 ng·ml^{-1}), glucose (10 mM), Glut-i (WZB 117 at 10 μM) in MCOs at 48 h. (B) Densitometry analysis of respective proteins was performed using ImageJ software and the respective fold change was written below each gel; ($n \geq 3$). Data represented as Mean ± S.E.M. from three independent experiments; $^{*}p < 0.05$, $^{**}p < 0.01$, $^{***}p < 0.001$ compared with respective vehicle; other comparison, $^{\wedge\wedge}p < 0.01$, $^{\wedge\wedge\wedge}p < 0.001$, $^{\#\#}p < 0.01$, $^{\#\#\#}p < 0.001$.

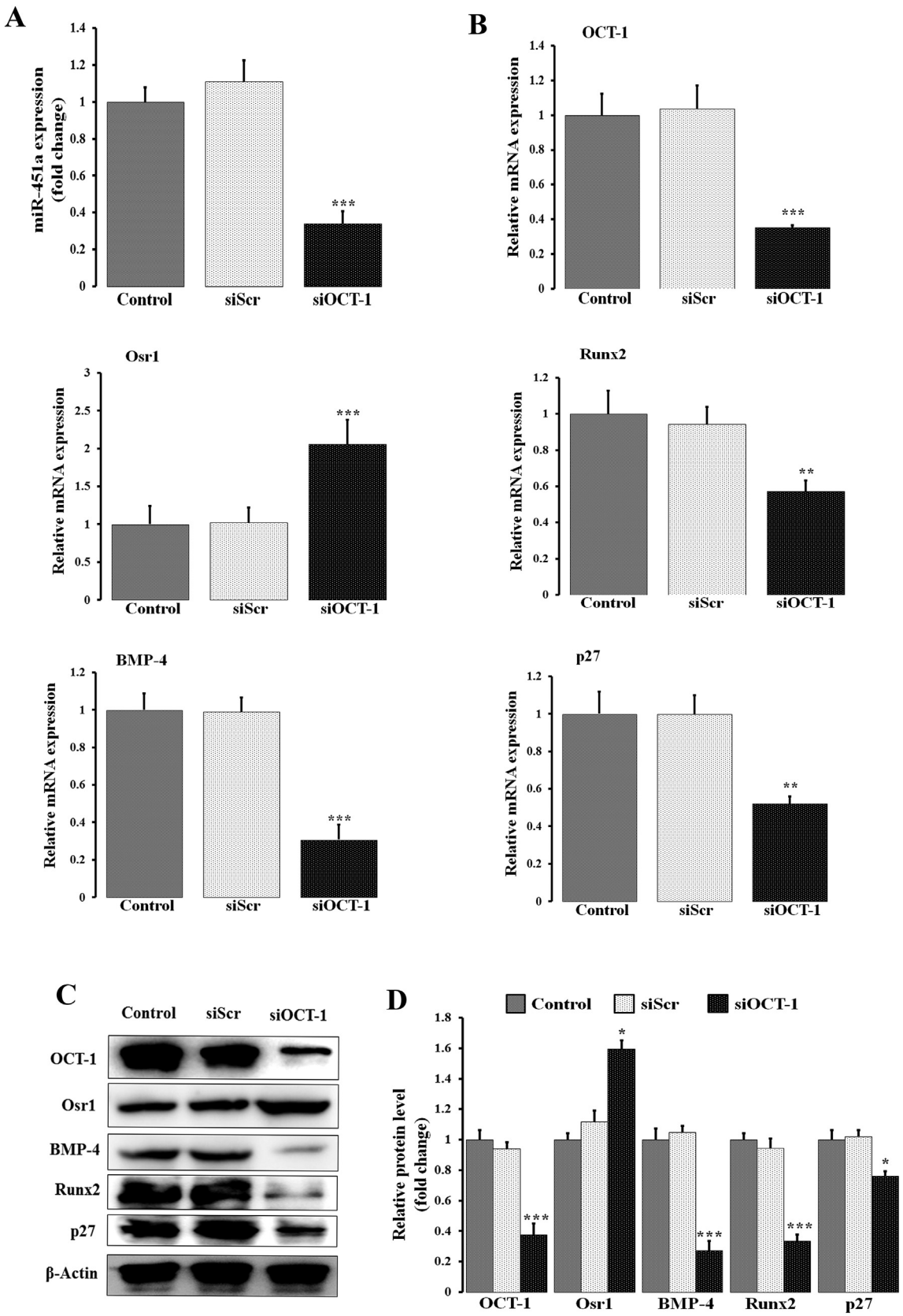

Fig. 5. OCT-1 drives miR-451a expression and promotes osteoblast differentiation. (A-D) Knockdown experiments in osteoblasts with siRNA against OCT-1 or scrambled siRNA (50 nM each) for expression (qPCR) of miR-451a after transfection in MCOs. ($n \geq 3$). (A); Quantitative PCR was performed for the expression of target gene Osr1, Runx2, BMP-4, and p27. ($n \geq 3$). (B); western blotting (C) and densitometry (D) respectively. ($n \geq 3$). Data represented as Mean ± S.E.M. from three independent experiments; $^{*}p < 0.05$, $^{**}p < 0.01$, $^{***}p < 0.001$ compared with respective vehicle.

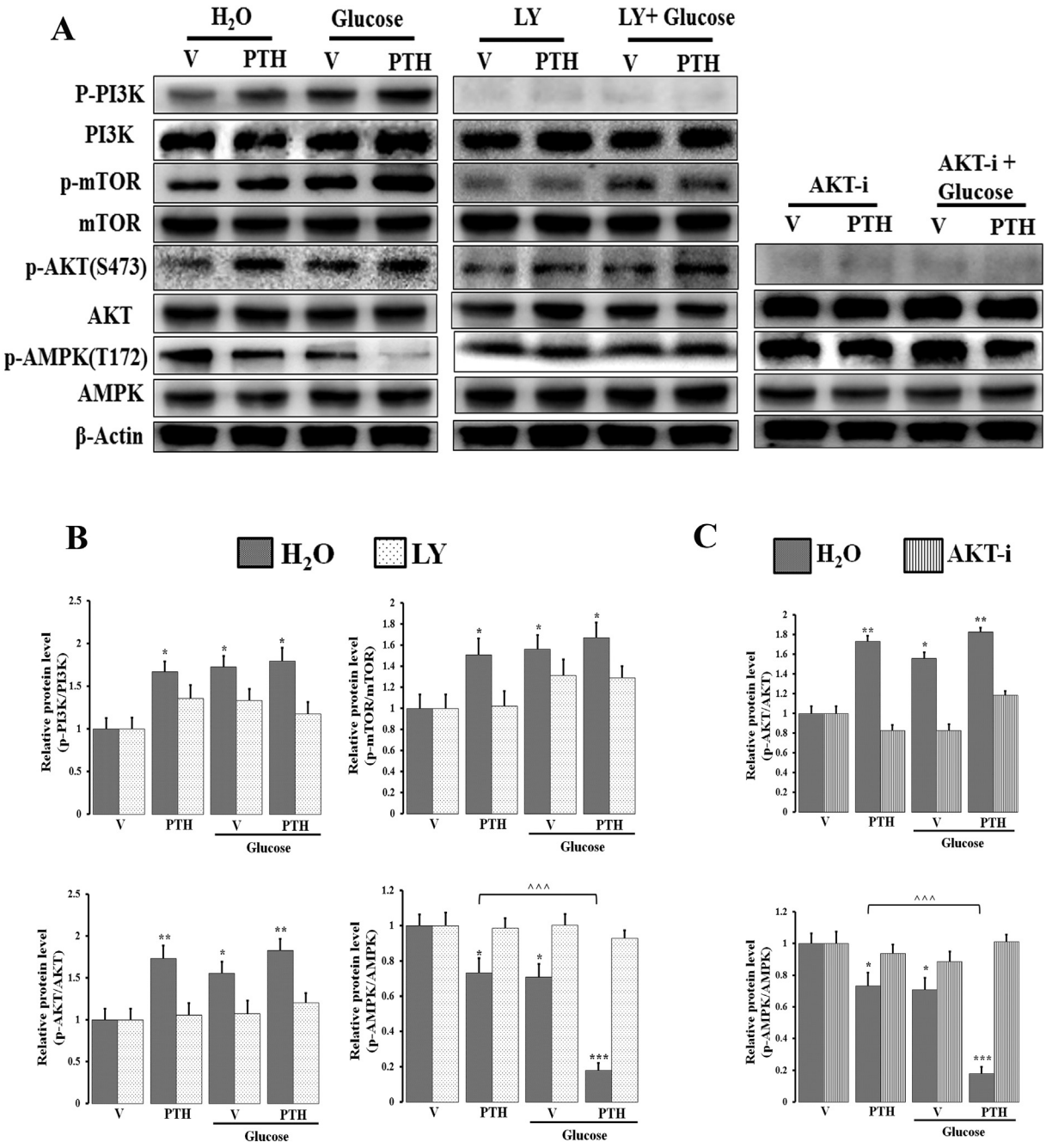

Fig. 6. PTH promotes glucose mediated inhibition of AMPK activation by PI3K-mTOR signaling. (A; left and middle panel) Western blotting and quantification were performed to assess the expression of a phosphorylated and non-phosphorylated form of PI3K, mTOR, AKT and AMPK with or without PTH (500 ng·ml^{-1}), glucose (10 mM), LY294002 (10 μM) in MCOs at 48 h; ($n \geq 3$). (C, right panel) Western blotting was performed to assess the expression of a phosphorylated and non-phosphorylated form of AKT and AMPK with or without PTH (500 ng·ml^{-1}), glucose (10 mM), AKT 1/2 inhibitor (10 μM) in MCOs at 48 h. ($n \geq 3$). Data represented as Mean ± S.E.M. from three independent experiments; Mean ± S.E.M.; *$p < 0.05$, **$p < 0.01$, ***$p < 0.001$ compared with respective vehicle; another comparison, ^^^$p < 0.001$.

appears to promote glucose uptake thereby inhibiting phosphorylation of AMPK through PI3K-mTOR-AKT signaling.

3.7. PTH promotes miR-451a expression in ovariectomized mice

Further, *in vivo* efficacy of PTH in regulating miR-451a levels was evaluated in ovariectomized mice. Similar to the previous study, we observed that PTH at 40 μg·kg^{-1} recovered bone loss [33] that happened due to ovariectomy (data not shown). In agreement to the *in vitro* results, PTH treatment for 6 weeks stimulated miR-451a expression in long bones both in sham (~5 to 6 fold) and Ovx (~3 to 4 fold) operated groups compared to respective vehicle treated groups (Fig. 7A). Moreover, PTH treatment reduced the Osr1 protein level and increased BMP-4, p27 and Runx2 protein levels in long bones as compared with Ovx animals (Fig. 7B). Immunohistochemical analysis further confirmed that PTH treatment reduced Osr1 and increased Runx2 protein levels in decalcified sections of distal femur metaphysis region (Fig. 7C).

Furthermore, we assessed protein levels in femur bone from these sham + V, Ovx + V and Ovx + PTH treatment groups. Consistent with *in vitro* data, PTH treatment to Ovx animals promoted p-PI3K, p-mTOR, p-AKT (S473) levels and reduced the p-AMPK (T172) and p-OCT (S336) levels compared to the Ovx + vehicle group (Fig. 7D–E). These findings

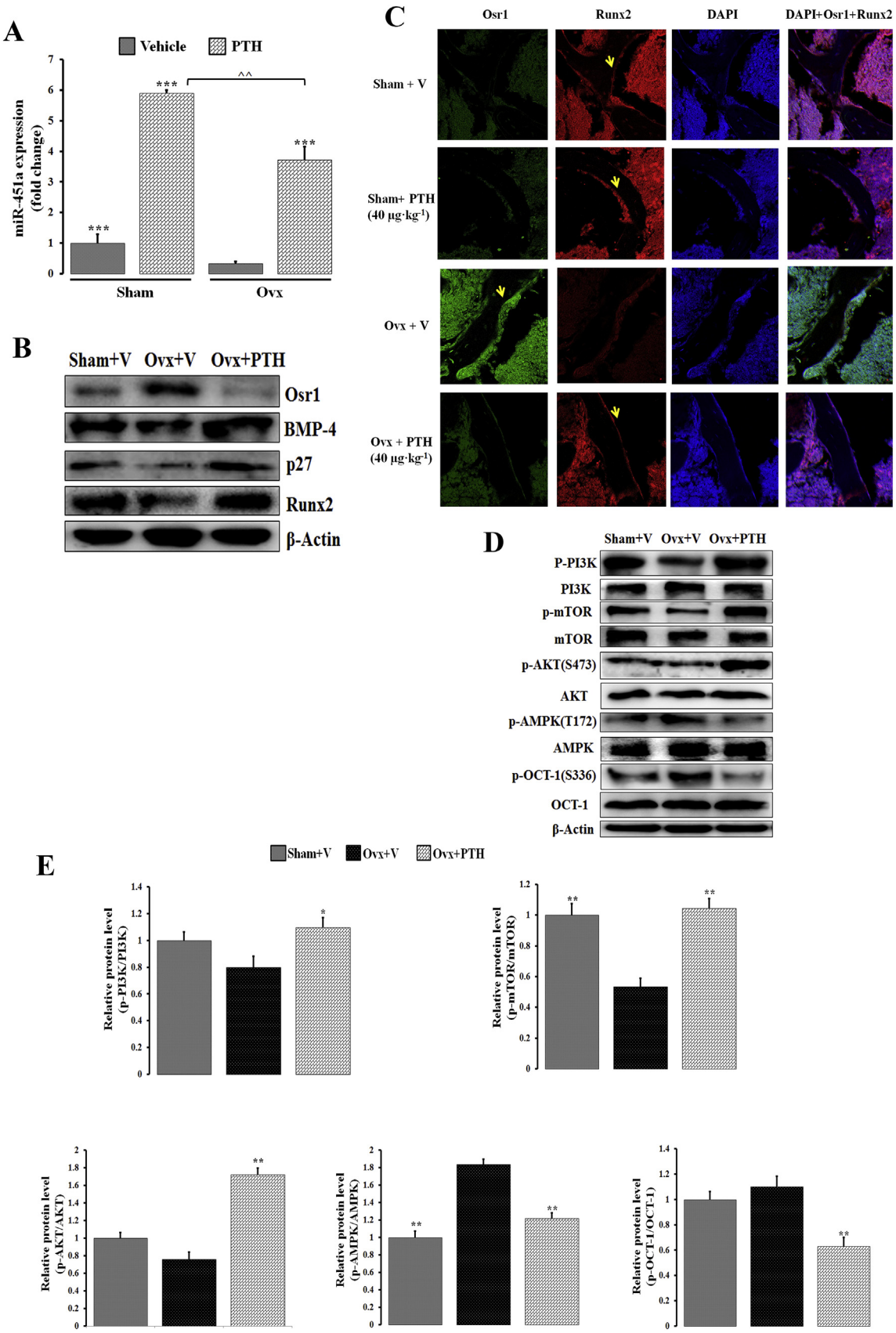

Fig. 7. PTH promotes miR-451a expression in ovariectomized mice. (A) Expression (qPCR) of miR-451a from femur, (B) western blotting showing the expression of target protein Osr1 and BMP-4, p27 and Runx2 at 48 h, (C) Immunofluorescence in decalcified sections for Osr1(Dilution 1:100) and Runx2 (Dilution 1:100), magnification-10× (4× zoom) in distal femur metaphysis, (D) Western blotting and quantification were performed to assess the expression of phosphorylated and non-phosphorylated form of PI3K, mTOR, AKT, AMPK and OCT-1 in femur bone from sham, sham + PTH (40 μg·kg^{-1}), ovariectomized and Ovx + PTH (40 μg·kg^{-1}) Balb/c mice, 8-week-old females; ($n = 6$). Data represented as Mean ± S.E.M. from three independent experiments; *$p < 0.05$, **$p < 0.01$, ***$p < 0.001$ compared with respective Ovx + vehicle group; other comparison, ^$p < 0.05$, ^^$p < 0.01$, ^^^$p < 0.001$.

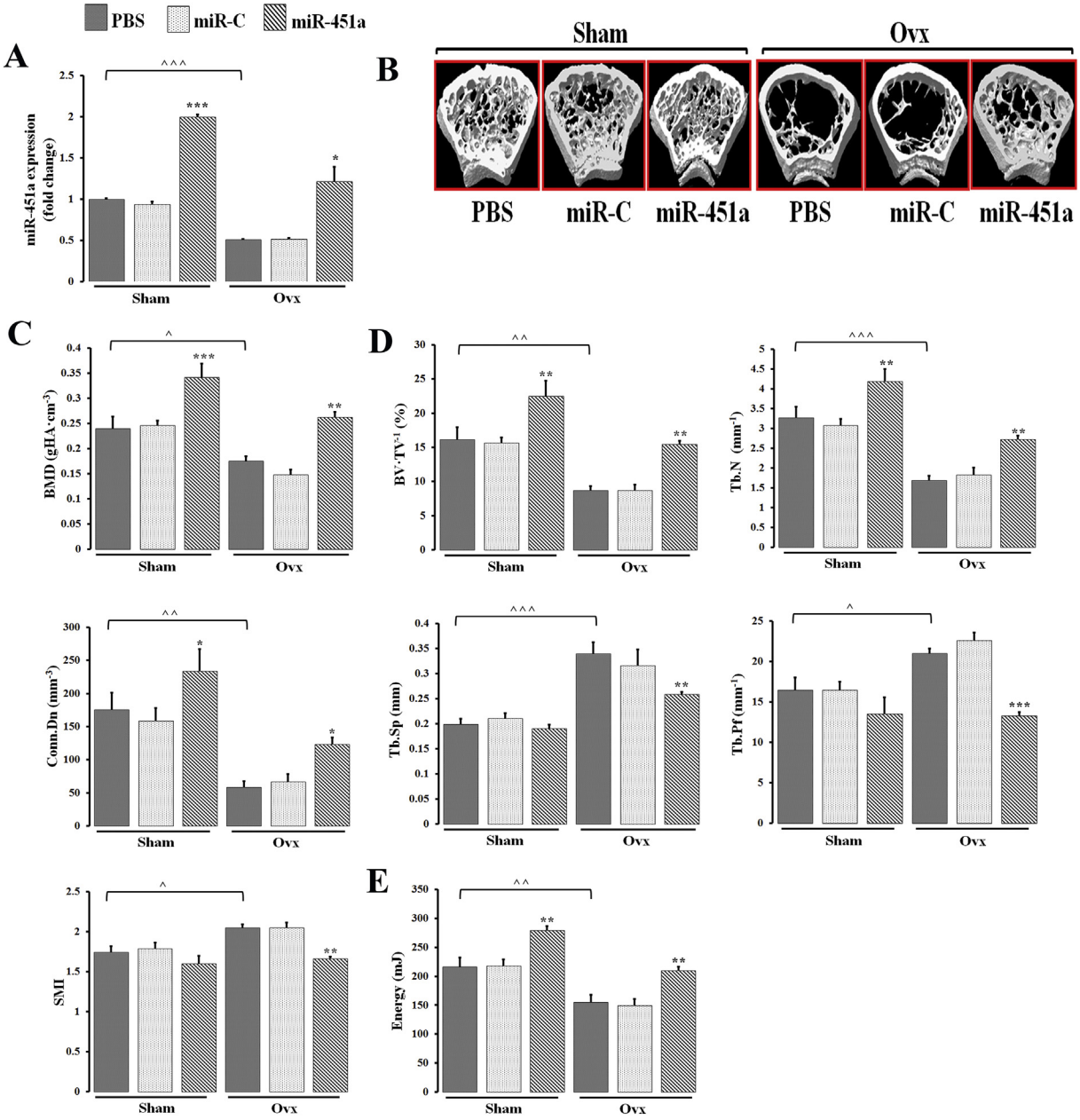

Fig. 8. miR-451a reverses ovariectomy-induced bone loss and improves strength in mice. (A) Enhanced miR-451a expression in bone following the injection of miR-451a (mimic) using Invivofectamine 3.0 Reagent into 8-week-old female Balb/c mice. This suggests adequate tissue uptake. (B) Representative μCT images of the distal femur metaphysis. (C) Bone mineral density; BMD, (D) structural μCT parameters, including bone volume-to-tissue volume; BV/TV, trabecular number; Tb.N, Connection density; Conn Dn, trabecular separation; Tb.Sp, Trabecular Pattern factor; Tb.Pf, Structural Model Index; SMI parameters (units shown) in femur metaphysis, (E) femoral bone strength shown by breaking energy (units are shown) from sham-operated (Sham) and ovariectomized (Ovx) mice that were given PBS (0.2 ml), scrambled miR (miR-C, 7 mg·kg^{-1}) or miR-451a (mimic, 7 mg·kg^{-1}) as indicated in the 'Results' section. Data represented as Mean ± S.E.M. from three independent experiments; *$p < 0.05$, **$p < 0.01$ and ***$p < 0.001$ compared with PBS-treated group; other comparison, ^$p < 0.05$, ^^$p < 0.01$ and ^^^$p < 0.001$ ($n = 6$ mice per group).

suggest that PTH promotes miR-451a expression and bone formation *in vivo*.

3.8. miR-451a shows anabolic action in ovariectomized mice

To address the anabolic function of miR-451a *in vivo*, ovariectomized and sham-operated mice were administered with the miR-451a mimic (7 mg·kg^{-1}) or scrambled miRNA (miR-C, 7 mg·kg^{-1}) or PBS (0.2 ml) for 6 weeks. Quantitative PCR assay confirmed the over-expression of miR-451a in femur bone extracts of both Sham and Ovx animals treated with miR-451a mimic. This confirmed effective *in vivo* tissue delivery and uptake of miR-451a (~2 fold) in both sham-operated and ovariectomized mice (Fig. 8A). We next evaluated the μCT parameters of trabecular bone at the distal femoral metaphysis. Fig. 8B shows representative images of the trabecular region of distal femur metaphysis. Ovariectomy expectedly reduced trabecular BMD, BV/TV, Tb.N, connection density while increased Tb.Sp, Tb.Pf and SMI. This significant trabecular loss was partially restored in miR-451a mimic treated animals; whereas miR-C and vehicle treated animals showed no such regain (Fig. 8C–D). Mimic treatment also prevented trabecular bone loss at both tibia and vertebra (Fig. S1). In addition, forced expression of miR-451a, increased femoral bone strength in both

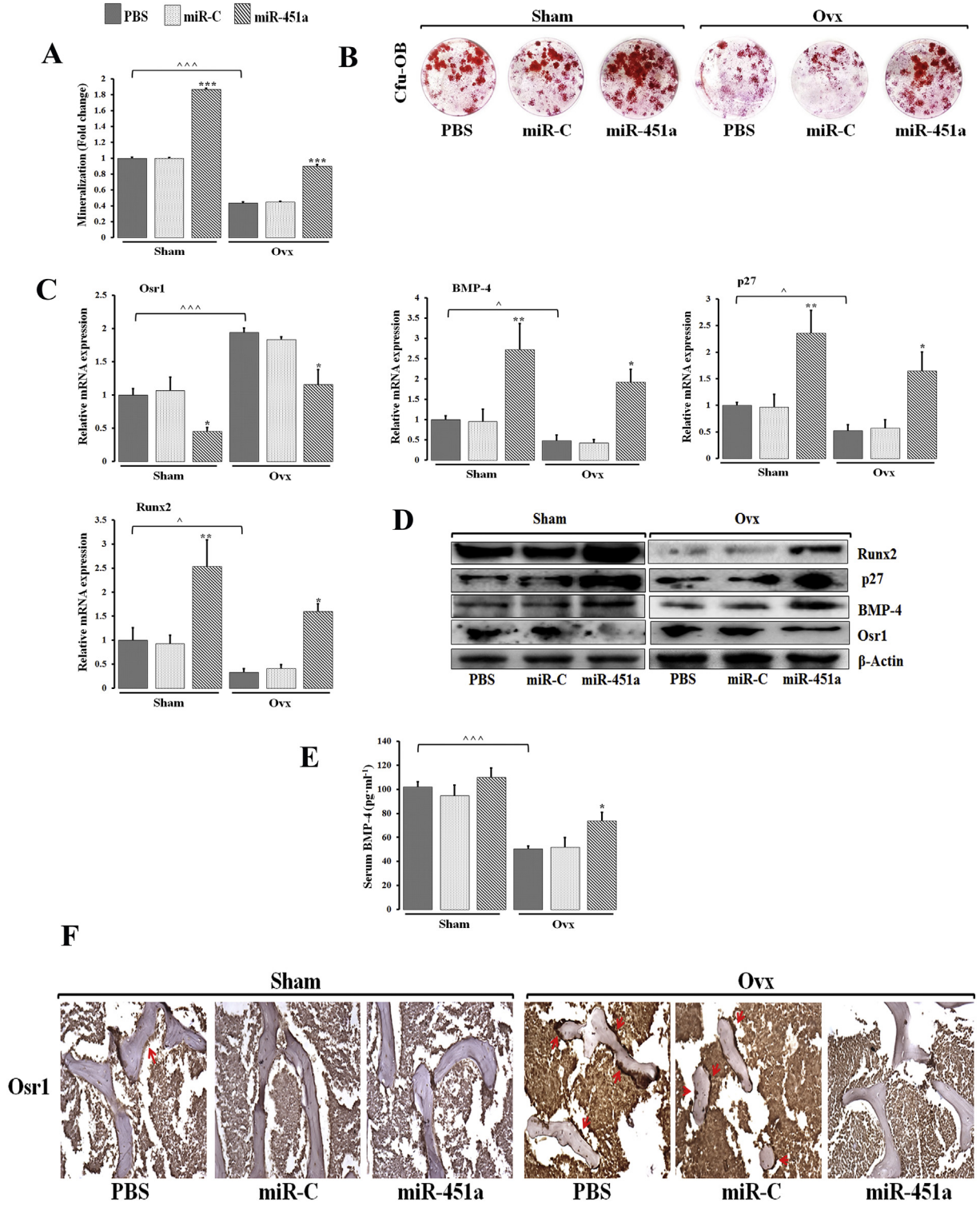

Fig. 9. miR-451a suppresses Osr1 *in vivo* to stimulate osteoblastogenesis. (A) *Ex vivo* BMCs culture showing mineralization, (B) representative wells showing alizarin-positive colony (Cfu-ob) formation in osteoblast cells cultures at day 15 in osteogenic medium, (C) qPCR and (D) western blotting analysis was performed for Osr1, BMP-4, p27 and Runx2, in femur bone, (E) serum BMP-4 levels ($pg{\cdot}ml^{-1}$) and (F) immunohistochemistry for Osr1 (magnification-20×) in distal femur metaphysis from sham-operated and ovariectomized mice that were given PBS (0.2 ml), scrambled miR (miR-C, 7 $mg{\cdot}kg^{-1}$) or miR-451a (mimic, 7 $mg{\cdot}kg^{-1}$) as indicated in the 'Results' section. Data represented as Mean ± S.E.M. from three independent experiments; ($n = 6$). *$p < 0.05$, **$p < 0.01$, ***$p < 0.001$ compared with PBS treated group; other comparisons, ^$p < 0.05$, ^^$p < 0.01$ and ^^^$p < 0.001$.

ovariectomized and sham-operated mice as significantly higher energy was required to break their bones then bones of miR-C and vehicle treated animals (Fig. 8E).

To further explore the mechanism of the increase in bone mass by overexpression of miR-451a, bone marrow stromal cells at 6 weeks were isolated. miR-451a mimic significantly increased mineralization and Cfu-ob formation compared with the control groups (Fig. 9A–B). Overall, miR-C administration did not affect these *ex vivo* parameters in

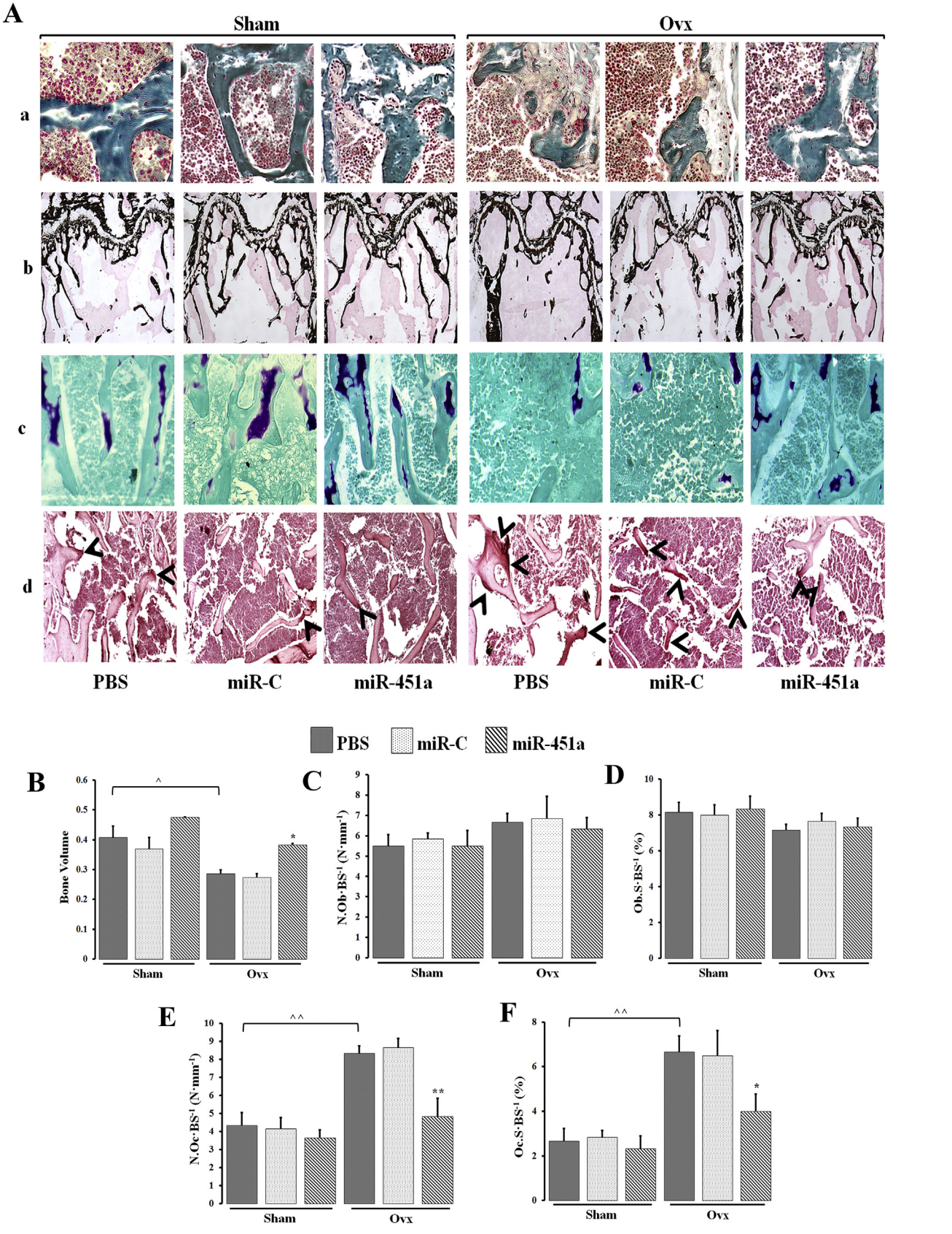

(caption on next page)

any of the group. Similar to *in vitro* transfection observations (Fig. 9J–L), mRNA and protein levels of BMP-4, p27 and Runx2 significantly increased and Osr1 levels decreased in bone extracts of mimic-treated mice compared with miR-C or PBS treated animals (Fig. 9C–D). Elevated serum BMP-4 levels were observed in miR-451a treatment groups confirming its bone anabolic effect (Fig. 9E).

Fig. 10. Histological examination of trabecular region of femur in both Sham and Ovx operated animals. (A) Goldner trichome staining (panel a) representing mineralized bone (magnification-20×) (A) Von Kossa staining (panel b) Toluidine blue staining (panel c) TRAP staining (panel d) (B–E) Total trabecular bone volume (B); N.Ob/BS, number of osteoblasts per bone surface (C); Ob.S/BS, osteoblast surface per bone surface (D); Corresponding parameters showed inhibited osteoclastogenesis and bone resorption in mimic treated mice. N.Oc/BS, number of osteoclasts per bone surface (E), Oc.S/BS, osteoclast surface per bone surface (F). in distal femur metaphysis from sham-operated and ovariectomized mice that were given PBS (0.2 ml), scrambled miR (miR-C, 7 mg·kg^{-1}) or miR-451a (mimic, 7 mg·kg^{-1}) as indicated in the 'Results' section. Data represented as Mean ± S.E.M. from three independent experiments; ($n = 6$). *$p < 0.05$ and **$p < 0.01$ compared with PBS treated group; other comparisons, ^$p < 0.05$ and ^^$p < 0.01$.

Immunohistochemistry results also showed that mimic-treatment suppressed the Osr1 levels both in Sham and Ovx group (Fig. 9F). Von Kossa and Toluidine blue staining revealed sparse and discontinuous trabeculae near the distal femur metaphysis were observed in Ovx mice (Fig. 10A). Mimic treatment to Ovx animals restored distorted trabecular microarchitecture. Bone histomorphometry analysis by Goldner trichome staining showed improvement in the trabecular bone volume of mimic-treated Sham and Ovx animals compared to PBS and miR-C treated groups (Fig. 10B). No changes in number of osteoblast per bone surface (N.Ob/BS) and percentage of surface covered by osteoblasts (Ob.S/BS) were observed in both Sham and Ovx operated groups (Fig. 10C–D). On the contrary ovariectomy resulted in bone resorption, as indicated by elevated the number of osteoclasts (OCs) per bone surface (N.Oc/BS) and the higher percentage of surfaces covered by OCs (Oc.S/BS) than sham operated mice. Mimic treatment to Ovx mice significantly reduced the N.Oc/BS and Oc.S/BS compared to miR-C and PBS treated Ovx mice (Fig. 10E–F). Overall, these data suggest that the *in vivo* anabolic action of miR-451a is mediated through Osr1 repression and Runx2 activation.

4. Discussion

This study showed an important role for PTH in regulating glucose dependent miR-451a expression during bone anabolism. We showed that PTH favors upregulation of miR-451a *via* increased glucose uptake leading to osteoblast differentiation. Our data demonstrated that PTH regulates glucose dependent miR-451a expression *via* the PI3K-mTOR-AKT-AMPK mechanism. Furthermore, we established the uncharacterized role of miR-451a during osteoblast differentiation, consistent with existing knowledge [42–44]. Maintenance of renal calcium and a moderate rise in PTH levels after weaning might be the reason behind post weaning bone recovery [14,15,45]. Considering that this miRNA is elevated during late weaning period [16], it is possible that it plays a key role in skeletal recovery following pregnancy and lactation in mother.

Previous studies have reported the contribution of several miRNAs, such as miR-26a, -133, -135, -29b, -2861, -3960 and -874-3p in the osteoblast differentiation [16,46–49]. Based on the earlier findings regarding PTH mediated glucose metabolism [8,10] and miR-451a dependency on glucose availability [22,23], we deciphered the connecting link between PTH and glucose controlled miR-451a expression during osteoblast differentiation. To elucidate the functional aspect of miR-451a related to PTH-stimulated osteoblast differentiation, we used mouse calvarial osteoblasts. In our study, we investigated the expression profile of miR-451a in various tissues. In mouse tissues, miR-451a was preferentially expressed in bone and liver and was detected at a lower level in muscle. Indeed, we found that PTH stimulates miR-451a expression in bone tissue. This finding may explain the possibility of a rise in miR-451a levels after PTH treatment in the prevention of fracture incidence, reliable with previous studies [1,20]. We found the expression of miR-451a is stage specific in osteoblast cells; miR-451a levels were high during differentiation and mineralization stages and were low during the proliferation stage. The key finding of our study is that miR-451a regulates osteoblast differentiation and function by suppressing its conserved target Osr1, which encodes a zinc-finger transcription factor that plays important roles in embryonic, kidney, heart, urogenital development and bone [50–52] and is active during osteoblast proliferative stage [52]. The functional role of miR-451a was further confirmed by overexpression and knockdown experiments. Therefore, we tested directly the modulatory effect of miR-451a expression, using specifically designed mimics and inhibitors (or Anti-miRs). Of note is that miR-451a has been characterized as a tumor-suppressive miRNA in osteosarcoma [17–19]. We found that transfection of osteoblast precursors with the miR-451a mimic stimulated cells to differentiate faster into mature, mineralizing osteoblasts and that this effect was associated with elevated BMP-4, p27 and Runx2 expression, consistent with previous studies [9,53,54]. Moreover, transfection experiments with miR-451a mimic showed a significant increase in osteoblast differentiation marker ALP and promoted bone mineralization *in vitro*. Furthermore, a consequence of mimic induced osteoblast differentiation and Runx2 expression were both dependent on Osr1 repression. This is not unexpected because there is prior evidence for an interaction between Osr1 and Runx2 where they experience inverse relation [55] and Osr1 is found to repress osteoblast differentiation [51,52]. Of note is our finding that BMP-4 expression is also regulated similarly, as Osr1 is known to negatively regulate BMP-4 expression levels [56]. Referring to previous knowledge, BMP-4 stimulates osteoblast differentiation and bone formation through enhancing p27 [53,54]. We found that miR-451a mimic stimulated BMP-4 expression both *in vitro* and *in vivo*. Therefore, we hypothesize that the inhibition of Osr1 by miR-451a increases Runx2 levels, potentiating BMP-4 induced osteoblast differentiation.

Osteoblasts undergo a developmental sequence of growth and differentiation characterized by a stage-specific expression of cell growth and bone-related genes. For this osteoblast requires glucose as a source of energy [57,58]. Here, we found glucose dose dependently stimulated miR-451a expression in osteoblasts, consistent with existing findings from hepatocytes and cancer cells [21,23,40]. Time and duration of exposure of glucose affected miR-451a levels. Similarly, PTH promoted glucose uptake and dose dependently upregulated miR-451a levels in osteoblasts *in vitro*. *In vivo* results confirmed the effect, where intermittent PTH treatment to Ovx Balb/c mice upregulated miR-451a levels in long bones. Assessment of miR-451a target protein Osr1 and bone related markers from PTH treated mice confirmed the stimulatory effect of PTH on miR-451a levels in bone.

Altered glucose metabolism in bone is associated with increased risk of bone disorders [59]. Previous study has shown that insulin and glucose elevate hepatic miR-451a levels and contribute to lower blood glucose levels in type 2 diabetes [40]. In addition to this, activation of AMPK levels and inhibition of osteoblast differentiation are dependent on glucose availability [9,60]. However, osteoblast differentiation requires a reduction in AMP kinase activity and glucose uptake by osteoblasts has shown to suppress AMPK activity. Notably, Activated AMPK is found to promote proteasomal degradation of Runx2 and thus hampers osteoblast differentiation [9,60]. Moreover, AMPK activation by glucose deprivation has been shown to inactivate OCT-1 *via* direct phosphorylation at serine 335, thus inhibiting miR-451a transcription in glioblastoma [23]. However, the same effect is unknown in bone tissue. To this effect, we report that pharmacological inhibition and activation of AMPK in osteoblasts lead to upregulation and down-regulation of miR-451a indicated by decreased and increased Osr1 levels respectively. PTH is known to stimulate aerobic glycolysis under the regulation of IGF-PI3K-mTOR-AKT mechanism [10]. Additionally, AKT is known to negatively regulate AMPK in the heart [61] and in the

later stages of osteoblast differentiation [62]. Hence, whether the same mechanism plays a role in PTH driven miR-451a expression in differentiating osteoblasts was checked. Here we found, pharmacological suppression of PI3K-mTOR-AKT signaling blunts PTH mediated miR-451a upregulation indicated by the elevated Osr1 and activated AMPK levels, thus alleviating the osteoblast differentiation function of PTH *in vitro*.

Extensive research has indicated that estrogen deficiency is the major cause of post-menopausal bone loss [63]. In addition, estrogen has been reported to positively regulate miR-451a in splenic lymphocytes [64,65]. Thus, we explored *in vivo* efficacy of miR-451a in 8-week-old ovariectomized mice which showed severe estrogen deficiency [16]. Mice were injected with mimic or scrambled miRNA intermittently over 6 weeks [16]. Mimic treatment prevented trabecular bone loss and improved bone strength both in ovariectomized mice and the sham-operated group. The *ex vivo* cultures of bone marrow stromal cells from mimic treated mice showed evidence of increased osteoblastogenesis, mineralization, and BMP-4 and Runx2 expression as well as reduced Osr1, essentially confirming our *in vitro* data. Bone histomorphometric analysis showed increased mineralized trabecular bone after the miR-451a treatment. Therefore, these findings document miR-451a as a potential anabolic target.

Overall we conclude, in the presence of glucose, inhibition of AMPK by PTH drives OCT-1 mediated miR-451a transcription leading to osteoblast differentiation *via* direct targeting of Osr1. The work not only clears and expands the remarkable studies about the effect of PTH on osteoblasts but more importantly provides evidence for the existence of additional regulatory mechanism behind PTH regulated osteoblast differentiation.

Conflict of interest

The authors have no conflict of interest.

Author's contributions

RT and AK designed this study. AK, PK, NA, SA, PK, AKT and VK performed experiments. RT and AK designed the experiments. All authors analyzed the data. Experiments were performed under the supervision of RT. RT and AK wrote the manuscript.

Acknowledgements

We gratefully acknowledge the Council of Scientific and Industrial Research (CSIR) India for the financial support from BSC0201 (ASTHI-Anabolic Skeletal Targets in Health and Illness) and BSC0111 (INDEPTH-Integrated NextGen Approaches in Disease and Environmental Toxicity). We are thankful to Council of Scientific and Industrial Research (CSIR) and University Grant Commission (UGC), New Delhi, India for the award of research fellowships. We thank to Dr. Dean Tantin, (University of Utah,) for gifting anti-phospho-OCT1 (S335) antibody. We acknowledge Dr. Kavita Singh of EM unit of CSIR-CDRI for collecting images of confocal microscopy data reported in this paper and Dr. Kalyan Mitra for facilitating confocal imaging.

Appendix A. Supplementary data

Trabecular assessment of μCT parameters in V^{th} lumbar vertebrae and tibia of both sham and ovariectomized mice underwent various treatments and calcein labeling in femur diaphysis (Fig. S1). Serum PINP levels (Fig. S2). Confocal imaging was performed to check BMP-4 expression after transfection experiment in MCOs (Fig. S3). Haematoxylin and eosin staining was performed for 5 μM transverse sections of kidney, liver and uterus for histology (Fig. S4). Supplementary data to this article can be found online at https://doi.org/10.1016/j.bone.2018.09.007.

References

[1] A.B. Hodsman, D.C. Bauer, D.W. Dempster, L. Dian, D.A. Hanley, S.T. Harris, D.L. Kendler, M.R. McClung, P.D. Miller, W.P. Olszynski, E. Orwoll, C.K. Yuen, Parathyroid hormone and teriparatide for the treatment of osteoporosis: a review of the evidence and suggested guidelines for its use, Endocr. Rev. 26 (5) (2005) 688–703.
[2] R.L. Jilka, Molecular and cellular mechanisms of the anabolic effect of intermittent PTH, Bone 40 (6) (2007) 1434–1446.
[3] T. Bellido, A.A. Ali, L.I. Plotkin, Q. Fu, I. Gubrij, P.K. Roberson, R.S. Weinstein, C.A. O'Brien, S.C. Manolagas, R.L. Jilka, Proteasomal degradation of Runx2 shortens parathyroid hormone-induced anti-apoptotic signaling in osteoblasts. A putative explanation for why intermittent administration is needed for bone anabolism, J. Biol. Chem. 278 (50) (2003) 50259–50272.
[4] S.W. Kim, P.D. Pajevic, M. Selig, K.J. Barry, J.Y. Yang, C.S. Shin, W.Y. Baek, J.E. Kim, H.M. Kronenberg, Intermittent parathyroid hormone administration converts quiescent lining cells to active osteoblasts, J. Bone Miner. Res. 27 (10) (2012) 2075–2084.
[5] H. Dobnig, R.T. Turner, Evidence that intermittent treatment with parathyroid hormone increases bone formation in adult rats by activation of bone lining cells, Endocrinology 136 (8) (1995) 3632–3638.
[6] S. Kimura, T. Sasase, T. Ohta, E. Sato, M. Matsushita, Parathyroid hormone (1–34) improves bone mineral density and glucose metabolism in spontaneously diabetic Torii-Lepr(fa) rats, J. Vet. Med. Sci. 74 (1) (2012) 103–105.
[7] P. D'Amelio, F. Sassi, I. Buondonno, E. Spertino, C. Tamone, S. Piano, D. Zugna, L. Richiardi, G.C. Isaia, Effect of intermittent PTH treatment on plasma glucose in osteoporosis: a randomized trial, Bone 76 (2015) 177–184.
[8] E. Zoidis, C. Ghirlanda-Keller, C. Schmid, Stimulation of glucose transport in osteoblastic cells by parathyroid hormone and insulin-like growth factor I, Mol. Cell. Biochem. 348 (1–2) (2011) 33–42.
[9] J. Wei, J. Shimazu, M.P. Makinistoglu, A. Maurizi, D. Kajimura, H. Zong, T. Takarada, T. Lezaki, J.E. Pessin, E. Hinoi, G. Karsenty, Glucose uptake and Runx2 synergize to orchestrate osteoblast differentiation and bone formation, Cell 161 (7) (2015) 1576–1591.
[10] E. Esen, S.Y. Lee, B.M. Wice, F. Long, PTH promotes bone anabolism by stimulating aerobic glycolysis via IGF signaling, J. Bone Miner. Res. 30 (11) (2015) 2137.
[11] G. Lombardi, C. Di Somma, L. Vuolo, E. Guerra, E. Scarano, A. Colao, Role of IGF-I on PTH effects on bone, J. Endocrinol. Investig. 33 (7 Suppl) (2010) 22–26.
[12] D.D. Bikle, T. Sakata, C. Leary, H. Elalieh, D. Ginzinger, C.J. Rosen, W. Beamer, S. Majumdar, B.P. Halloran, Insulin-like growth factor I is required for the anabolic actions of parathyroid hormone on mouse bone, J. Bone Miner. Res. 17 (9) (2002) 1570–1578.
[13] H.J. Kalkwarf, B.L. Specker, Bone mineral loss during lactation and recovery after weaning, Obstet. Gynecol. 86 (1) (1995) 26–32.
[14] N.A. Cross, L.S. Hillman, S.H. Allen, G.F. Krause, Changes in bone mineral density and markers of bone remodeling during lactation and postweaning in women consuming high amounts of calcium, J. Bone Miner. Res. 10 (9) (1995) 1312–1320.
[15] N.A. Cross, L.S. Hillman, S.H. Allen, G.F. Krause, N.E. Vieira, Calcium homeostasis and bone metabolism during pregnancy, lactation, and postweaning: a longitudinal study, Am. J. Clin. Nutr. 61 (3) (1995) 514–523.
[16] P. Kushwaha, V. Khedgikar, D. Sharma, T. Yuen, J. Gautam, N. Ahmad, A. Karvande, P.R. Mishra, P.K. Trivedi, L. Sun, S.K. Bhadada, M. Zaidi, R. Trivedi, MicroRNA 874-3p exerts skeletal anabolic effects epigenetically during weaning by suppressing Hdac1 expression, J. Biol. Chem. 291 (8) (2016) 3959–3966.
[17] J. Yuan, J. Lang, C. Liu, K. Zhou, L. Chen, Y. Liu, The expression and function of miRNA-451 in osteosarcoma, Med. Oncol. 32 (1) (2015) 324.
[18] H. Xu, Q. Mei, L. Shi, J. Lu, J. Zhao, Q. Fu, Tumor-suppressing effects of miR451 in human osteosarcoma, Cell Biochem. Biophys. 69 (1) (2014) 163–168.
[19] W. Liu, S.Y. Liu, Y.B. He, R.L. Huang, S.Y. Deng, G.X. Ni, B. Yu, MiR-451 suppresses proliferation, migration and promotes apoptosis of the human osteosarcoma by targeting macrophage migration inhibitory factor, Biomed Pharmacother 87 (2017) 621–627.
[20] T. Waki, S.Y. Lee, T. Niikura, T. Iwakura, Y. Dogaki, E. Okumachi, K. Oe, R. Kuroda, M. Kurosaka, Profiling microRNA expression during fracture healing, BMC Musculoskelet. Disord. 17 (2016) 83.
[21] J. Godlewski, A. Bronisz, M.O. Nowicki, E.A. Chiocca, S. Lawler, microRNA-451: a conditional switch controlling glioma cell proliferation and migration, Cell Cycle 9 (14) (2010) 2742–2748.
[22] J. Godlewski, M.O. Nowicki, A. Bronisz, G. Nuovo, J. Palatini, M. De Lay, J. Van Brocklyn, M.C. Ostrowski, E.A. Chiocca, S.E. Lawler, MicroRNA-451 regulates LKB1/AMPK signaling and allows adaptation to metabolic stress in glioma cells, Mol. Cell 37 (5) (2010) 620–632.
[23] K.I. Ansari, D. Ogawa, A.K. Rooj, S.E. Lawler, A.M. Krichevsky, M.D. Johnson, E.A. Chiocca, A. Bronisz, J. Godlewski, Glucose-based regulation of miR-451/AMPK signaling depends on the OCT1 transcription factor, Cell Rep. 11 (6) (2015) 902–909.
[24] B. Gamez, E. Rodriguez-Carballo, R. Bartrons, J.L. Rosa, F. Ventura, MicroRNA-322 (miR-322) and its target protein Tob2 modulate Osterix (Osx) mRNA stability, J. Biol. Chem. 288 (20) (2013) 14264–14275.
[25] A. Grimson, K.K. Farh, W.K. Johnston, P. Garrett-Engele, L.P. Lim, D.P. Bartel, MicroRNA targeting specificity in mammals: determinants beyond seed pairing, Mol. Cell 27 (1) (2007) 91–105.
[26] B. John, A.J. Enright, A. Aravin, T. Tuschl, C. Sander, D.S. Marks, Human microRNA targets, PLoS Biol. 2 (11) (2004) e363.
[27] T. Ishizuya, S. Yokose, M. Hori, T. Noda, T. Suda, S. Yoshiki, A. Yamaguchi,

Parathyroid hormone exerts disparate effects on osteoblast differentiation depending on exposure time in rat osteoblastic cells, J. Clin. Invest. 99 (12) (1997) 2961–2970.
[28] C.A. Gregory, W.G. Gunn, A. Peister, D.J. Prockop, An Alizarin red-based assay of mineralization by adherent cells in culture: comparison with cetylpyridinium chloride extraction, Anal. Biochem. 329 (1) (2004) 77–84.
[29] A. Karvande, V. Khedgikar, P. Kushwaha, N. Ahmad, P. Kothari, A. Verma, P. Kumar, G.K. Nagar, P.R. Mishra, R. Maurya, R. Trivedi, Heartwood extract from *Dalbergia sissoo* promotes fracture healing and its application in ovariectomy-induced osteoporotic rats, J. Pharm. Pharmacol. 69 (10) (2017) 1381–1397.
[30] E.E. Beier, T.J. Sheu, E.A. Resseguie, M. Takahata, H.A. Awad, D.A. Cory-Slechta, J.E. Puzas, Sclerostin activity plays a key role in the negative effect of glucocorticoid signaling on osteoblast function in mice, Bone Res. 5 (2017) 17013.
[31] V. Khedgikar, P. Kushwaha, J. Gautam, A. Verma, B. Changkija, A. Kumar, S. Sharma, G.K. Nagar, D. Singh, P.K. Trivedi, N.S. Sangwan, P.R. Mishra, R. Trivedi, Withaferin A: a proteasomal inhibitor promotes healing after injury and exerts anabolic effect on osteoporotic bone, Cell Death Dis. 4 (2013) e778.
[32] K.V. Sashidhara, S.P. Singh, S. Varshney, M. Beg, A.N. Gaikwad, Poliothrysoside and its derivatives as novel insulin sensitizers potentially driving AMPK activation and inhibiting adipogenesis, Eur. J. Med. Chem. 86 (2014) 570–577.
[33] A. Iida-Klein, H. Zhou, S.S. Lu, L.R. Levine, M. Ducayen-Knowles, D.W. Dempster, J. Nieves, R. Lindsay, Anabolic action of parathyroid hormone is skeletal site specific at the tissue and cellular levels in mice, J. Bone Miner. Res. 17 (5) (2002) 808–816.
[34] J. Kureel, M. Dixit, A.M. Tyagi, M.N. Mansoori, K. Srivastava, A. Raghuvanshi, R. Maurya, R. Trivedi, A. Goel, D. Singh, miR-542-3p suppresses osteoblast cell proliferation and differentiation, targets BMP-7 signaling and inhibits bone formation, Cell Death Dis. 5 (2014) e1050.
[35] J.Y. Yang, S.W. Cho, J.H. An, J.Y. Jung, S.W. Kim, S.Y. Kim, J.E. Kim, C.S. Shin, Osteoblast-targeted overexpression of TAZ increases bone mass in vivo, PLoS One 8 (2) (2013) e56585.
[36] C.H. Hu, B.D. Sui, F.Y. Du, Y. Shuai, C.X. Zheng, P. Zhao, X.R. Yu, Y. Jin, miR-21 deficiency inhibits osteoclast function and prevents bone loss in mice, Sci. Rep. 7 (2017) 43191.
[37] S.F. Li, J.J. Tang, J. Chen, P. Zhang, T. Wang, T.Y. Chen, B. Yan, B. Huang, L. Wang, M.J. Huang, Z.M. Zhang, D.D. Jin, Regulation of bone formation by baicalein via the mTORC1 pathway, Drug Des. Devel. Ther. 9 (2015) 5169–5183.
[38] C. Li, S. Hao, H. Wang, L. Jin, F. Qing, F. Zheng, P. Zhang, L. Chen, D. Ma, T. Zhang, MicroRNA expression profiling and target genes study in congenital microtia, Int. J. Pediatr. Otorhinolaryngol. 77 (4) (2013) 483–487.
[39] F. Morandi, V. Pistoia, Soluble HLA-G modulates miRNA-210 and miRNA-451 expression in activated CD4+ T lymphocytes, Int. Immunol. 25 (5) (2013) 279–285.
[40] S. Zhuo, M. Yang, Y. Zhao, X. Chen, F. Zhang, N. Li, P. Yao, T. Zhu, H. Mei, S. Wang, Y. Li, S. Chen, Y. Le, MicroRNA-451 negatively regulates hepatic glucose production and glucose homeostasis by targeting glycerol kinase-mediated gluconeogenesis, Diabetes 65 (11) (2016) 3276–3288.
[41] X. Liu, R.R. Chhipa, I. Nakano, B. Dasgupta, The AMPK inhibitor compound C is a potent AMPK-independent antiglioma agent, Mol. Cancer Ther. 13 (3) (2014) 596–605.
[42] L. He, G.J. Hannon, MicroRNAs: small RNAs with a big role in gene regulation, Nat. Rev. Genet. 5 (7) (2004) 522–531.
[43] V. Ambros, The functions of animal microRNAs, Nature 431 (7006) (2004) 350–355.
[44] Y. Zhao, D. Srivastava, A developmental view of microRNA function, Trends Biochem. Sci. 32 (4) (2007) 189–197.
[45] G.N. Kent, R.I. Price, D.H. Gutteridge, M. Smith, J.R. Allen, C.I. Bhagat, M.P. Barnes, C.J. Hickling, R.W. Retallack, S.G. Wilson, et al., Human lactation: forearm trabecular bone loss, increased bone turnover, and renal conservation of calcium and inorganic phosphate with recovery of bone mass following weaning, J. Bone Miner. Res. 5 (4) (1990) 361–369.
[46] E. Luzi, F. Marini, S.C. Sala, I. Tognarini, G. Galli, M.L. Brandi, Osteogenic differentiation of human adipose tissue-derived stem cells is modulated by the miR-26a targeting of the SMAD1 transcription factor, J. Bone Miner. Res. 23 (2) (2008) 287–295.
[47] Z. Li, M.Q. Hassan, S. Volinia, A.J. van Wijnen, J.L. Stein, C.M. Croce, J.B. Lian, G.S. Stein, A microRNA signature for a BMP2-induced osteoblast lineage commitment program, Proc. Natl. Acad. Sci. U. S. A. 105 (37) (2008) 13906–13911.
[48] Z. Li, M.Q. Hassan, M. Jafferji, R.I. Aqeilan, R. Garzon, C.M. Croce, A.J. van Wijnen, J.L. Stein, G.S. Stein, J.B. Lian, Biological functions of miR-29b contribute to positive regulation of osteoblast differentiation, J. Biol. Chem. 284 (23) (2009) 15676–15684.
[49] R. Hu, W. Liu, H. Li, L. Yang, C. Chen, Z.Y. Xia, L.J. Guo, H. Xie, H.D. Zhou, X.P. Wu, X.H. Luo, A Runx2/miR-3960/miR-2861 regulatory feedback loop during mouse osteoblast differentiation, J. Biol. Chem. 286 (14) (2011) 12328–12339.
[50] R.G. James, C.N. Kamei, Q. Wang, R. Jiang, T.M. Schultheiss, Odd-skipped related 1 is required for development of the metanephric kidney and regulates formation and differentiation of kidney precursor cells, Development 133 (15) (2006) 2995–3004.
[51] S. Stricker, S. Mathia, J. Haupt, P. Seemann, J. Meier, S. Mundlos, Odd-skipped related genes regulate differentiation of embryonic limb mesenchyme and bone marrow mesenchymal stromal cells, Stem Cells Dev. 21 (4) (2012) 623–633.
[52] S. Kawai, M. Yamauchi, A. Amano, Zinc-finger transcription factor Odd-skipped related 1 regulates cranial bone formation, J. Bone Miner. Metab. (2017), https://doi.org/10.1007/s00774-017-0885-9 [Epub ahead of print].
[53] S.F. Chang, T.K. Chang, H.H. Peng, Y.T. Yeh, D.Y. Lee, C.R. Yeh, J. Zhou, C.K. Cheng, C.A. Chang, J.J. Chiu, BMP-4 induction of arrest and differentiation of osteoblast-like cells via p21 CIP1 and p27 KIP1 regulation, Mol. Endocrinol. 23 (11) (2009) 1827–1838.
[54] A. Yamaguchi, T. Ishizuya, N. Kintou, Y. Wada, T. Katagiri, J.M. Wozney, V. Rosen, S. Yoshiki, Effects of BMP-2, BMP-4, and BMP-6 on osteoblastic differentiation of bone marrow-derived stromal cell lines, ST2 and MC3T3-G2/PA6, Biochem. Biophys. Res. Commun. 220 (2) (1996) 366–371.
[55] M. Yamauchi, S. Kawai, T. Kato, T. Ooshima, A. Amano, Odd-skipped related 1 gene expression is regulated by Runx2 and Ikzf1 transcription factors, Gene 426 (1–2) (2008) 81–90.
[56] S.A. Rankin, A.L. Gallas, A. Neto, J.L. Gomez-Skarmeta, A.M. Zorn, Suppression of Bmp4 signaling by the zinc-finger repressors Osr1 and Osr2 is required for Wnt/beta-catenin-mediated lung specification in Xenopus, Development 139 (16) (2012) 3010–3020.
[57] J.B. Lian, G.S. Stein, The developmental stages of osteoblast growth and differentiation exhibit selective responses of genes to growth factors (TGF beta 1) and hormones (vitamin D and glucocorticoids), J. Oral. Implantol. 19 (2) (1993) 95–105 (discussion 136-7).
[58] A. Mobasheri, Glucose: an energy currency and structural precursor in articular cartilage and bone with emerging roles as an extracellular signaling molecule and metabolic regulator, Front. Endocrinol. (Lausanne) 3 (2012) 153.
[59] C.M. Karner, F. Long, Glucose metabolism in bone, Bone 115 (2018) 2–7.
[60] T. Kasai, K. Bandow, H. Suzuki, N. Chiba, K. Kakimoto, T. Ohnishi, S. Kawamoto, E. Nagaoka, T. Matsuguchi, Osteoblast differentiation is functionally associated with decreased AMP kinase activity, J. Cell. Physiol. 221 (3) (2009) 740–749.
[61] S. Kovacic, C.L. Soltys, A.J. Barr, I. Shiojima, K. Walsh, J.R. Dyck, Akt activity negatively regulates phosphorylation of AMP-activated protein kinase in the heart, J. Biol. Chem. 278 (41) (2003) 39422–39427.
[62] G. Xi, C.J. Rosen, D.R. Clemmons, IGF-I and IGFBP-2 stimulate AMPK activation and autophagy, which are required for osteoblast differentiation, Endocrinology 157 (1) (2016) 268–281.
[63] B.L. Riggs, The mechanisms of estrogen regulation of bone resorption, J. Clin. Invest. 106 (10) (2000) 1203–1204.
[64] R. Dai, R.A. Phillips, Y. Zhang, D. Khan, O. Crasta, S.A. Ahmed, Suppression of LPS-induced interferon-gamma and nitric oxide in splenic lymphocytes by select estrogen-regulated microRNAs: a novel mechanism of immune modulation, Blood 112 (12) (2008) 4591–4597.
[65] R. Dai, S. McReynolds, T. Leroith, B. Heid, Z. Liang, S.A. Ahmed, Sex differences in the expression of lupus-associated miRNAs in splenocytes from lupus-prone NZB/WF1 mice, Biol. Sex Differ. 4 (1) (2013) 19.